Understanding in situ ozone production in the summertime through radical observations and modelling studies during the Clean air for London project (ClearfLo)

Lisa K. Whalley[1,2], Daniel Stone[1], Rachel Dunmore[3], Jacqueline Hamilton[3], James R. Hopkins[3,4], James D. Lee[3,4], Alistair C. Lewis[3,4], Paul Williams[5,6], Jörg Kleffmann[7], Sebastian Laufs[7], Robert Woodward-Massey[1] & Dwayne E. Heard[1,2]

[1] School of Chemistry, University of Leeds, Leeds, LS2 9JT, UK
[2] National Centre for Atmospheric Science, University of Leeds, Leeds, LS2 9JT, UK
[3] Department of Chemistry, University of York, York, YO10 5DD, UK
[4] National Centre for Atmospheric Science, University of York, YO10 5DD, UK
[5] Centre for Atmospheric Sciences, School of Earth, Atmospheric & Environmental Sciences, University of Manchester, Manchester, M13 9PL, UK
[6] National Centre for Atmospheric Sciences, University of Manchester, Manchester, M13 9PL, UK
[7] Institute for Atmospheric & Environmental Research, Bergische Universität Wuppertal (BUW), Gaußstr. 20, 42119 Wuppertal, Germany

Correspondence to: Lisa K. Whalley (l.k.whalley@leeds.ac.uk) and Dwayne E. Heard (d.e.heard@leeds.ac.uk)

Abstract. Measurements of OH, HO_2, RO_2i (alkene and aromatic related RO_2) and total RO_2 radicals taken during the ClearfLo campaign in central London in the summer of 2012 are presented. A photostationary steady-state calculation of OH which considered measured OH reactivity as the OH sink term and the measured OH sources (of which HO_2+NO reaction and HONO photolysis dominated) compared well with the observed levels of OH. Comparison with calculations from a detailed box model utilising the Master Chemical Mechanism v3.2, however, highlighted a substantial discrepancy between radical observations under lower NO_x conditions ([NO] < 1 ppbv) typically experienced during the afternoon hours, and indicated that the model was missing a significant peroxy radical sink; the model over-predicted HO_2 by up to a factor of 10 at these times. Known radical termination steps, such as HO_2 uptake on aerosols, were not sufficient to reconcile the model measurement discrepancies alone suggesting other missing termination processes. This missing sink was most evident when the air reaching the site had previously passed over central London to the east and when elevated temperatures were experienced and, hence, contained higher concentrations of VOC. Uncertainties in the degradation mechanism at low NO_x of complex biogenic and diesel related VOC species which were particularly elevated and dominated OH reactivity under these easterly flows, may account for some of the model measurement disagreement. Under higher [NO] (>3 ppbv) the box model increasingly under-predicted total [RO_2]. The modelled and observed HO_2 were in agreement, however, under elevated NO concentrations ranging from 7 – 15 ppbv.

The model uncertainty under low NO conditions leads to more ozone production predicted using modelled peroxy radical concentrations (~3 ppbv hr^{-1}) versus ozone production from peroxy radicals measured (~1 ppbv hr^{-1}). Conversely, ozone production derived from the predicted peroxy radicals is up to an order of magnitude lower than from the observed peroxy radicals as [NO] increases beyond 7 ppbv due to the model under-prediction of RO_2 under these conditions.

5 1 Introduction

With greater than 50 % of the global population residing in urban conurbations, poor urban air quality has a demonstrable effect on human health. OH and HO_2 radicals, (collectively termed HO_x) together with RO_2 radicals, mediate virtually all of the oxidative chemistry in the atmosphere. The hydroxyl radical initiates the removal of primary emissions, including toxic gases such as CO and benzene, leading to the formation of peroxy radicals which, in the presence of NO, form secondary
10   pollutants such as NO_2, O_3 and particulates. Public Health England (2014) reports that pollutants contribute to 29,000 deaths a year in the UK, with a reduction in life expectancy (by an average of 6 months) caused by the long-term exposure to pollutants, and the cost to society is estimated at up to £20 billion per year. In areas of London up to 1 in 12 deaths are at least partly attributable to air pollution, yet big uncertainties still remain relating to the chemistry, transformation and removal rate of primary emissions in large urban conurbations, meaning our ability to predict pollution episodes is compromised.

15   The EU air quality guidelines recommend that ozone concentrations do not exceed 60 ppbv for greater than an 8 hour period (http://www.eea.europa.eu/themes/air/ozone), with a 10 ppbv increment in long term exposure to ozone increasing the risk of death from respiratory causes by ~ 3 – 4% (Jerrett et al., 2009). Short-term exposure to elevated levels of tropospheric ozone have been associated with several adverse health effects including, for example, exacerbation of asthma in children (Thurston et al., 1997).

20   Despite successful reductions in many ozone precursors across Europe, ozone levels have increased at certain urban sites due to the long-term decrease in NO_x emissions. For example, Bigi and Harrison (2010) report a steady increase in ozone between 1996-2008 in North Kensington; an urban background site in London.

To implement efficient reduction strategies for ozone, a detailed understanding of the factors controlling free radicals is critical since the reaction of HO_2 and RO_2 radicals with NO, forming NO_2, followed by the subsequent photolysis of NO_2 represents
25   the only net formation pathway to tropospheric ozone:

$$OH + RH\ (+O_2) \rightarrow RO_2 + H_2O \tag{R1}$$

$$NO + RO_2 \rightarrow NO_2 + RO \tag{R2}$$

$$RO + O_2 \rightarrow R_{-H}O + HO_2 \tag{R3}$$

$$NO + HO_2 \rightarrow NO_2 + OH \tag{R4}$$

$$NO_2 + h\nu \rightarrow NO + O \tag{R5}$$

$$O + O_2 \xrightarrow{M} O_3 \tag{R6}$$

$$NO + O_3 \rightarrow NO_2 + O_2 \tag{R7}$$
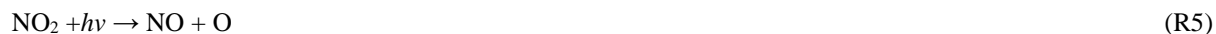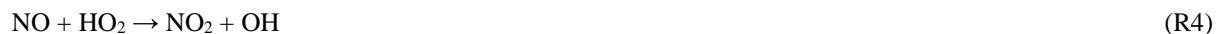
Measurements of radicals have been made at various urban and suburban locations worldwide, both during the summer and winter (Stone et al. (2012) and references therein). Observations of OH and HO_2 in the urban atmosphere have primarily been made using fluorescence assay by gas expansion (FAGE), and comparisons with predicted radical concentrations using chemistry box models constrained with co-located radical precursor measurements have revealed varying levels of success in replicating observations. Radical concentrations have been reported to be under-predicted by models (Ren et al., 2003; Martinez et al., 2003; Emmerson et al., 2005a; Chen et al., 2010; Lu et al., 2012; Lu et al., 2013), over-predicted (George et al., 1999; Konrad et al., 2003; Dusanter et al., 2009) and, at times, models and measurements have been reported to be in reasonable agreement, to within 40%, (Shirley et al., 2006; Emmerson et al., 2007; Kanaya et al., 2007; Sheehy et al., 2010; Elshorbany et al., 2012; Ren et al., 2013; Griffith et al., 2016). Often the level of agreement observed was found to be dependent on time of day (Brune et al., 2016); with poorest agreement between modelled and measured OH concentrations generally observed during the night. Griffith et al. (2016) found that the level of agreement between modelled and measured HO_2 was dependent on whether it was a weekday or weekend; the model under-predicted HO_2^* by a factor of 3.4 during the week when NO mixing ratio were greater than 4 ppbv but agreed well on weekends (observed to modelled $HO_2^* = 1.3$) when NO concentrations were below 4 ppbv. In a number of studies, the model-measurement discrepancy was noted to increase as NO_x levels increased beyond ~1 ppbv (Martinez et al., 2003; Ren et al., 2013; Brune et al., 2016). This increasing under-prediction of the free-radicals (particularly for HO_2) with increasing NO_x concentrations observed may reflect inaccuracies in the radical propagation steps in the model, which cycle HO_2 to OH. In light of the recently reported RO_2 interference suffered by FAGE (Fuchs et al., 2011; Whalley et al., 2013) when detecting HO_2, however, it is possible that the measured HO_2 under these conditions may have been increasingly influenced by the presence of RO_2 species. The extent of this interference will be dependent upon the level of interference suffered by the specific FAGE instrument utilised and the concentration of those RO_2 species that interfere (principally aromatic, alkene and $>C_3$ alkane-derived RO_2 species) that were present in a particular environment. Similarly, two FAGE groups have reported interferences in their OH measurements made using wavelength modulation in the presence of ambient levels of ozone and alkenes (Mao et al., 2012; Novelli et al., 2014), whilst, in contrast, good agreement between OH measurements made using FAGE and differential optical absorption spectroscopy (DOAS) during chamber measurements suggests minimal interferences in the presence of ozone and alkenes for a third FAGE instrument (Fuchs et al., 2013). This lack of interference was further corroborated in recent laboratory tests (Fuchs et al., 2016) although an artefact signal under dark conditions (deriving from NO_3 in the presence of H_2O) was identified. These potential

artefacts make it difficult to identify trends in earlier model-measurement comparisons and to assess how well the models are performing under a range of chemical conditions. Some of the more recently published radical measurements at urban sites include corrections for OH interferences, e.g. (Ren et al., 2013; Brune et al., 2016; Griffith et al., 2016) and radical measurements from the MEGAPOLI project which took place at a suburban site close to Paris employed the chemical ionisation mass spectrometry (CIMS) technique to make observations of OH and the sum of HO_2 and RO_2 species rather than FAGE (Michoud et al., 2012). HO_2^* (= $[HO_2]$ +$\sum_i\alpha_i$ $[RO_2i]$, and α_i is the mean fractional contribution of the RO_2 species that interfere (RO_2i)) model-measurement comparisons are now often reported (rather than HO_2) to take into account contributions from RO_2 species (Lu et al., 2013; Griffith et al., 2016) and very recently Tan et al. (2017) presented interference-free HO_2 observations alongside RO_2 observations which were made using the FAGE technique coupled to a flow reactor (Fuchs et al., 2008) at a rural site in Wangdu, China. In contrast to some of the earlier HO_2 model-measurement comparisons which diverged at NO concentrations > 1ppbv with models increasingly under-predicting the levels of HO_2 observed, the predicted levels of HO_2 were in good agreement with HO_2 observations made in Wangdu over the whole range (0.1 – 4 ppbv) of NO encountered (Tan et al., 2017). However, the authors did report an increasing model under-prediction of the observed RO_2 with increasing NO (Tan et al., 2017).

Despite uncertainties in some of the earlier radical observations and discrepancies between observed and predicted radical concentrations, detailed modelling studies have demonstrated a number of common themes relevant to urban photochemistry:

1. The primary source of OH from the photolysis of ozone and subsequent reaction of the excited state oxygen atom with H_2O, which is often considered the dominant radical source in many other environments (e.g in the remote marine atmosphere (Whalley et al., 2010)) tends only to play a minor role in urban centres, with this source accounting for < 6% of the total radical sources during MCMA-2006 (Dusanter et al., 2009) which took place in Mexico City.

2. Owing to the prevalence of carbonyl and dicarbonyl species in the urban atmosphere, a number of studies have highlighted the role that the photolysis of these species play as key radical precursors (and, hence, ozone precursors) in the summertime: During the SHARP-2009 project that took place in Houston, Texas, the photolysis of formaldehyde accounted for 14% of radical production, with the photolysis of other OVOCs contributing a further 15% (Ren et al., 2013). During the CAREBeijing2006 HCHO was estimated to contribute ~30% to the overall radical production (Lu et al., 2013).

3. Ozonolysis reactions have been reported as important primary radical sources during a number of studies, for example these reactions accounting for 67% of the OH initiation in Birmingham during the PUMA campaign in winter (Emmerson et al., 2005b) whilst in Tokyo during the IMPACT campaign ozonolysis reactions were the dominant radical source during the night-time in winter (Kanaya et al., 2007).

4. The photolysis of HONO, which takes place at longer wavelengths than ozone photolysis, has been demonstrated to act as an important OH source in the morning (Kleffmann, 2007). At urban sites (including London), significant

concentrations of HONO (often several hundred pptv) have been reported to persist throughout the day (Lee et al., 2016), and, as such, HONO should be considered an important OH source throughout sunlit hours, not just at sunrise, in these environments. Dusanter et al. (2009) found that HONO photolysis contributed 35% of daytime HO_x production in Mexico City during MCMA 2006, whilst Tan et al. (2017) found that HONO photolysis was the most important primary radical source in Wangdu in the North China Plain.

There have now been several observations of total OH reactivity (k_{OH}) in urban environments. With some of the highest reactivities of >120 s^{-1} recorded in the megacities such as Mexico City, London and Paris. In many of the large cities (Houston, New York City, Mexico City), OH reactivity has been found to be dominated by anthropogenic hydrocarbons, CO and NO_x. OVOCs have been highlighted as significant OH sinks in a number of urban studies, contributing between 11–24% during summertime at these urban centres (Mao et al., 2010b), whilst we recently reported that the oxidation products of biogenic emissions contributed a significant fraction to the total OH reactivity observed in London (Whalley et al., 2016). A measurement of OH reactivity can provide an additional model target, with model-measurement comparisons helping identify unmeasured primary emissions or unmeasured oxidised intermediates which may promote radical propagation. Furthermore, when coupled with OH (and HO_2) observations, the closure of OH production (P_{OH}) and OH loss ($D_{OH} = k_{OH}[OH]$) terms can be critically assessed independent of a model. In an urban atmosphere the dominant OH sources include recycling from HO_2+NO, HONO photolysis, $O(^1D)$ (from ozone photolysis) +H_2O and ozonolysis reactions. In the recent study in the Wangdu region of China, P_{OH} was found to equal D_{OH} within uncertainties throughout the day (Tan et al., 2017) demonstrating consistency between the observed radical concentrations and observed OH reactivity (Fuchs et al., 2017). Several previous studies in urban regions, however, have found that P_{OH} is balanced by D_{OH} during the afternoon but not in the mornings, with measured P_{OH} approximately twice D_{OH} from sunrise to noon (Brune et al., 2016). This imbalance of P_{OH} and D_{OH} suggests either a negative bias of OH reactivity measurements, an error in the HO_2 measurement or uncertainties in the chemistry of other key OH sources, e.g. HONO (Brune et al., 2016).

Urban radical measurements can be used to estimate local ozone production (Kanaya et al., 2007; Ren et al., 2013; Brune et al., 2016) by approximating the rate of ozone production to the production rate of NO_2 from the reaction of NO with HO_2 and RO_2 radicals, and assuming instantaneous O_3 production following photolysis of NO_2 at wavelengths <400 nm. Any loss of NO_2 which does not yield O_3, for example the reaction of OH or RO_2 radicals with NO_2, and also deposition, should also be considered:

$$P(O_3) = (k_{HO_2+NO}[HO_2][NO] + k_{RO_2+NO}[RO_2][NO]) - (k_{OH+NO_2+M}[OH][NO_2][M] + k_{RO_2+NO_2+M}[RO_2][NO_2][M])$$

(1)

Given the short lifetime of the radicals, this estimate provides a method of gauging the extent to which the fast local chemistry influences the net ozone levels observed relative to O_3 generated during transport. A shortcoming of this approach in earlier studies is that often the RO_2 concentration used in E1 is estimated or modelled, as traditionally the FAGE technique measures OH and HO_2 only. In the Wangdu study, however, Tan et al., (2017) using observed RO_2 demonstrated that models may under-predict ozone production at high NO due to an underestimation of the RO_2 radical concentration.

In the present paper we utilise observations of OH and HO_2 radicals made using the FAGE technique and RO_2 radicals using the RO_xLIF method (Whalley et al., 2013). The radical observations were made during the Clean air for London project (ClearfLo) during the summer of 2012 and are used to directly determine local ozone production. To assess the factors controlling the radical budget and in turn ozone production, we have employed a detailed box model based on the MCM v3.2. By comparing model predictions to radical observations the key reactions taking place in London that are ultimately controlling the air quality are identified and uncertainties in our current understanding of urban oxidation chemistry is highlighted.

2 Experimental

2.1 Site description

The ClearfLo Intensive Operation Period (IOP) ran from 22nd July to 18th August and overlapped with the London 2012 summer Olympics. An extensive suite of instrumentation was deployed and operated from the grounds of Sion Manning School in North Kensington (51° 31'16" North, 0°12'48" West), which is located adjacent to a long-term air quality monitoring site in North Kensington (Bigi and Harrison, 2010). Further details on the campaign and location may be found in Bohnenstengel et al. (2015).

2.2 FAGE instrument description

The University of Leeds ground-based FAGE instrument was deployed to the North Kensington site and made measurements of OH, HO_2 and RO_2 radicals. Further details on the instrument for OH and HO_2 detection can be found in Whalley et al. (2010) with only an outline of the specific set-up and running conditions during ClearfLo described here. The radical measurements were made from a 20 ft air-conditioned shipping container which had been converted into a mobile laboratory. The instrument consists of two FAGE detection cells which were located on the roof of the shipping container, in a weather-proof housing, at a height of 3.5 m. A Nd:YAG pumped Ti:Sapphire laser (Photonics Industries) generated pulsed (repetition rate of 5 kHz), tunable near IR radiation, which was frequency doubled and tripled to provide UV light at 308 nm and was used to excite OH via the $Q_1(1)$ transition of the $A^2\Sigma^+$, v'=0 $\leftarrow$ $X^2\Pi_i$, v''=0 band. On-resonance fluorescence was detected using a gated channel photo-multiplier and photon counting for a period of 300 s. The laser was then scanned beyond the OH transition (by 0.004 nm) and a background signal collected for a further 75 s to determine the contribution of laser, solar scatter and detector noise to the total signal for subtraction (OH_{WAVE}).

In previous configurations, the two detection cells were used to simultaneously detect OH by laser-induced fluorescence (LIF) (cell 1) and HO_2 by NO titration to OH followed by LIF (cell 2). The UV laser light was split upon exiting the laser and focussed into fibre optics (5 m length) for delivery to each cell individually. During ClearfLo, the two cells were coupled together via a connecting side arm, which enabled light exiting cell 1 to pass into cell 2, and meant that light previously needed for the detection of HO_2 in cell 2 could be used for other applications (for example OH reactivity measurements, as was the case during this deployment (Stone et al., 2016)). As in previous configurations, the light exiting the fibre optic passed through a collimator coupled to a baffled entrance arm, this arrangement produced a beam profile of ~ 1 cm diameter which remained well collimated as it passed through both cells. A UV anti-reflective coated window was placed in the centre of the connecting arm to effectively seal the cells from each other. A further modification to the previously deployed configuration involved the coupling of a flow reactor to detection cell 2 to enable an RO_2 radical measurement. Further details on this approach are outlined below. Consequently, cell 1 was used for sequential measurements of OH and HO_2, with NO (BOC, 99.5%) injected into this cell during the second half of the online detection period.

2.3 ROx-LIF description

An 83 cm long, 6.4 cm internal diameter flow reactor was coupled vertically to the second FAGE detection cell to facilitate detection of RO_2 radicals by LIF using the approach described by Fuchs et al. (2008). This flow reactor was held at approximately 30 Torr, with ~7.5 SLM ambient air drawn into the reactor via a 1 mm diameter pinhole. The flow reactor was operated in two modes. In the first, referred to as the HO_x mode, 250 sccm CO (BOC, 5% in N_2) was mixed with the ambient air close to the inlet to promote conversion of ambient OH to HO_2. In the second, referred to as the RO_x mode, 25 sccm of NO in N_2 (BOC, 500 ppmv) was also added to the CO flow which led to conversion of RO_2 to OH. The CO present rapidly reconverted any OH formed (or any OH sampled) to HO_2. Air (5 SLM) sampled by the flow reactor was transferred into the FAGE fluorescence detection cell (which was held at ~1.5 Torr) via a 4 mm diameter pinhole. 100 sccm NO (BOC, 99.5%) was injected into the fluorescence cell, converting HO_2 to OH for subsequent detection by LIF. In RO_x mode a measure of OH+HO_2+sum of RO_2 was obtained.

In laboratory tests, the relative sensitivity of the instrument to a range of different RO_2 species was investigated (see Table 1). Similar sensitivities were determined for the RO_2 species tested, therefore, we use the assumption that under ambient conditions individual RO_2 species are converted and, hence, detected with the same efficiency as methane-derived RO_2 radicals. The same assumption was drawn in the recent RO_x study in Wangdu, China (Tan et al., 2017). This assumption means that the concentration of RO_2 observed may be a lower estimate as certain RO_2 species will not convert as efficiently as methane-derived RO_2 radical. For example, the MCM predicts that only ~ 20% of NO_3-adduct RO_2 radicals which derive from the reaction of simple alkenes (e.g. ethene and propene) with NO_3 will convert to HO_2 in the presence of NO at the reduced pressures of the flow reactor and so we expect RO_xLIF to have low sensitivity to these RO_2 types.

2.4 Calibration

The instrument was calibrated twice weekly on average using photolysis of a known concentration of water vapour at 185 nm within a turbulent flow tube to generate OH and HO_2, with the product of the photon flux at 185 nm and the water vapour photolysis time measured using a chemical actinometer (Commane et al., 2010). For RO_2, methane (BOC, CP grade, 99.5%) was added to the humidified air flow in sufficient quantity to rapidly convert OH to CH_3O_2. The limit of detection (LOD) at a signal-to-noise ratio of one for one data acquisition cycle lasting 7 minutes was $\sim 4.5 \times 10^5$ molecule cm^{-3} for OH, $\sim 2.1 \times 10^6$ molecule cm^{-3} for HO_2 and $\sim 6.9 \times 10^6$ molecule cm^{-3} for CH_3O_2 at a typical laser power of 13 mW in each cell. The measurements were recorded with 1 s time-resolution, and the accuracy of the measurements was $\sim$ 26 % (2σ).

2.5 Potential radical artefacts and corrections

2.5.1 OH

A small OH artefact signal (OH_{INT}) which derives from photolysis of O_3 by the 308 nm laser light, followed by the abstraction of an H atom from H_2O vapour within the FAGE cell, has been observed in laboratory tests. Such an artefact has been observed in other FAGE systems (Griffith et al., 2016; Fuchs et al., 2016; Tan et al., 2017), and although the reported magnitude of the interference is variable for different systems, the signal scales linearly with both O_3 and H_2O and displays a quadratic dependence with laser power. The following correction has been applied to the OH data presented here which corresponds to 5.2×10^5 molecule cm^{-3} of OH at 50 ppbv O_3, 2% H_2O and 10 mW laser power (determined after the campaign but under the same experimental conditions):

$$OH_{RAW\ CORR} = OH_{RAW\ OBS} - OH_{INT} \tag{2}$$

where:

$$OH_{INT}\ (\text{molecule } cm^{-3}) = 520\ (\pm 200) \times [O_3]\ (\text{ppbv}) \times [H_2O]\ (\%) \times \text{Laser power (mW)} \tag{3}$$

It should be noted that in later laboratory tests on the Leeds FAGE system with a modified nozzle design, the determined OH_{INT} was slightly lower than reported here. Fuchs et al. (2016) also report a variable artefact signal for the Jülich FAGE system. This variability introduces a high level of uncertainty into this correction. The OH_{INT} presented here should likely be considered an upper limit as any increase in the magnitude of this correction would lead to negative OH concentrations calculated during night-time periods.

Along with full characterisation of the O_3-H_2O OH artefact signal, the Leeds FAGE system has subsequently been characterised with respect to other potential artefact signals, for example, an artefact deriving from reaction products of ozone and alkenes. Furthermore, in the most recent field campaigns, an inlet pre injector (IPI) has been used to chemically scavenge

ambient OH, and provides an alternative method to determine background signals (to generate OH_{CHEM}) alongside the wavelength tuning approach discussed above (OH_{WAVE}). The laboratory interference tests and field comparison of OH_{CHEM} and OH_{WAVE} in different environments will be subject of a future publication (Woodward-Massey et al., in preparation). In general, however, good agreement between OH_{CHEM} and OH_{WAVE} has been observed for the Leeds FAGE instrument (including during ambient measurements conducted in another urban environment in central Beijing with an OH_{WAVE} to OH_{CHEM} ratio of 1.04 and 1.07 in winter and summer respectively (Woodward-Massey et al., 2017)) and no significant artefact signal was observed in the interference tests conducted to date providing confidence in the OH measurements presented here.

2.5.2 HO_2 and RO_2i

Fuchs et al., (2011) and later Whalley et al., (2013) identified that specific RO_2 radical classes (primarily those derived from alkene and aromatic hydrocarbons, defined here as RO_2i) have the potential to decompose to OH in the presence of NO under typical FAGE cell conditions and, as a result, may be classed as an HO_2 interference. Depending on the type of FAGE cell and pressures employed, and NO concentration used, the level of interference can be deliberately varied (Whalley et al., 2013). During ClearfLo, two different NO concentrations (1.0 and 9.0×10^{13} molecule cm^{-3}) were introduced into cell 1 to promote detection of (a) mainly HO_2 under low concentrations of added NO, and (b) $HO_2 + RO_2i$ under high concentrations of added NO. With knowledge of the sensitivity to HO_2 and RO_2i at the two added NO concentrations, determined by adding a known concentration of HO_2 and ethene-derived RO_2 during calibration, and using the methodology outlined in Whalley et al., (2013), the concentration of RO_2i and interference-free HO_2 can be determined. In the following Results and Discussions we compare RO_2i derived from measurements using $\alpha_i = 0.72 \pm 0.09$ and $\alpha_i = 0.19 \pm 0.09$ at the high and low NO flow respectively to modelled RO_2i.

2.5.3 RO_2

Fuchs et al. (2008) described the potential of peroxy nitric acid and methyl peroxy nitric acid, HO_2NO_2 and $CH_3O_2NO_2$, (the concentration of which will be most elevated at high NO_x) to thermally decompose in the RO_x-LIF flow reactor. In this urban setting, the RO_2 signal that we attribute solely to non-interfering RO_2 species (RO_2ni) (determined by subtracting $HO_2 + RO_2i$ measured in cell 1 from the total RO_2 signal measured by RO_xLIF in RO_x mode) may also include a contribution from $CH_3O_2NO_2$. Here, we refer to the measurement of non-interfering RO_2 species (RO_2ni) which includes a contribution from the thermal decomposition of $CH_3O_2NO_2$ as RO_2ni^*. If the concentration of RO_2ni is dominated by CH_3O_2, it is possible to estimate the ambient concentration of $CH_3O_2NO_2$ from the radical measurements themselves and, thus, make a correction for this artefact without relying on model predictions of $CH_3O_2NO_2$. The methodology for this correction is outlined in the SI along with the RO_2ni data corrected for this potential artefact. Owing to the unknown fraction of the total RO_2ni that is CH_3O_2, we have left the data uncorrected in sections 3 and 4 below. It is worth noting, however, that this correction is most significant

when NO concentrations peak during the morning; a time (as discussed in section 3.3.2) when the RO_2ni observations are under-estimated by model predictions.

2.6 Model description

A zero dimensional box model based on the Master Chemical Mechanism (MCMv3.2) (Jenkin et al., 2012) was used to predict radical concentrations for comparison with those observed. Complete details of the kinetic and photochemical data used in the mechanism are available at the MCM website (http://mcm.leeds.ac.uk/MCM/home). The model was run with a sub-set of the MCM and treated the degradation of simultaneously measured trace VOCs, CH_4 and CO following oxidation by OH, O_3 and NO_3, and included ~15000 reactions and ~3800 species. The model was constrained by measurements of NO, NO_2, O_3, CO, CH_4, 62 individual VOC species measured by GC-FID and also 2D-GC PAN, HCHO, HNO_3, HONO, water vapour, temperature and pressure. The model was constrained with measured $j(O^1D)$, $j(NO_2)$, $j(HONO)$, $j(HCHO)$, $j(CH_3COCH_3)$ and $j(CH_3CHO)$ made using a spectral radiometer. For further instrumental details relating to all the model constraints please refer to Table 2 (and the references therein). For all other photo-labile species in the model, photolysis rates were scaled to the ratio of clear-sky $j(O^1D)$, calculated using a two-steam isotropic scattering model (Hayman, 1997), to observed $j(O^1D)$ to account for clouds. A constant H_2 concentration of 500 ppbv was assumed (Forster et al., 2012). The model inputs were updated every 15 minutes. For species measured more frequently, data were averaged to 15 minute intervals, whilst those measured at a lower time resolution were interpolated. The loss of all non-constrained, model generated, species by deposition or mixing was represented as a first order loss rate equivalent to 1 cm s^{-1} in a boundary layer depth which varied from ~300 m during the night to 1800 m in the afternoon (estimated from vertical velocity variance (Barlow et al., 2015)) leading to lifetimes of ~8 hrs during the night and ~ 50 hrs during the afternoons.

The model was run for the entirety of the campaign in overlapping 7 day segments. To allow all the unmeasured, model-generated intermediate species time to reach steady state concentrations, the model was initialised with inputs from the first measurement day (23rd July) and spun-up for 5 days before comparison to measurements were made. Comparison of these 5 spin-up days demonstrated that the concentration of model generated species rapidly converged and there was less than a 1% difference in (for example) modelled OH concentration by the second spin up day. As a result of this, the model segments were run so as to overlap for 2 days only to reduce the computing time.

In all model scenarios a first of loss (k'_{loss}) for HO_2 was included to represent heterogeneous removal (Ravishankara, 1997):

$$k'_{loss} = \frac{\omega A \gamma}{4} \tag{4}$$

where ω is the mean molecular speed of HO_2 (equal to 43725 cm s^{-1} at 298 K), γ is the aerosol uptake coefficient and A is the aerosol surface area density in cm^2 cm^{-3}. A is calculated using data from an aerodynamic particle sizer instrument (TSI Inc,

model 3321) which counts particles in 53 size bins ranging from 0.53 to 21.29 μm. For most of the scenarios considered γ was held constant at 0.1.

 A series of distinct model scenarios were simulated to assess the sensitivity of the modelled radical concentrations to a number of model parameters. In the following results and discussions the radical measurements are compared (for the most part) to the base model scenario (MCM-BASE) which was run with the constraints outlined above.

3 Results

3.1 Radical observations and model predictions during the summer ClearfLo IOP

Near continuous radical measurements were made in London, from 23rd July to 17th August 2012. Typically, winds from the south west, ranging from less than 1 ms^{-1} during the night to between $4 - 6$ ms^{-1} in the afternoon, were encountered. Close to the start of the campaign (24th – 27th July) and also later in the campaign (9th – 12th, 14th Aug), however, the wind direction switched to an easterly flow, bringing air that had passed over central London to the site, and wind speeds dropped. Fine weather prevailed during these easterly flows, with enhancements in air temperature and solar radiation (Fig. 1, top panel) observed. During these periods, radical concentrations (particularly the peroxy radicals) were elevated; the time-series of OH, HO$_2$, RO$_2$i, and the sum of RO$_2$ species (not including a HO$_2$ contribution) is presented in Figure 2. The concentration of a number of other species such as NO$_x$, CO and O$_3$ were also elevated (Fig. 1) during the easterly flows. Indeed, the concentration of the O$_3$ was observed to increase rapidly on the warmer days from sunrise, peaking during the afternoon at concentrations between 60 - 100 pbbv, and was found, on the 25th July, to exceed EU air quality recommendations of 60 ppbv for greater than a 6 hr period. The average diurnal profiles of the different radicals during south westerly and easterly flows are presented in Figure 3.

The short lifetime of OH (10 – 100 ms) measured directly in London from OH reactivity measurements (Whalley et al., 2016) dictates that OH exists in a photostationary steady state (PSS), where the rate of OH production is balanced by the rate of OH destruction (f is the fraction of O(^{1}D) that reacts with H$_2$O to form OH):

$$[OH]_{PSS} = \frac{\sum k \times [OH_{source}]}{\sum k \times [OH_{sink}]} = \frac{P_{OH}}{k_{OH}} \tag{5}$$

$$[OH]_{PSS} = \frac{\sum 2 j(O^1D)[H_2O][O_3]f + k_{HO_2+NO}[HO_2][NO] + j(HONO)[HONO] + ozonolysis}{k_{OH}} \tag{6}$$

[OH]$_{PSS}$ may be estimated from the rate of production from the sum of co-measured OH sources; here the rate of OH production from rate of reaction of HO$_2$ with NO, HONO photolysis, O$_3$ photolysis and the subsequent reaction of O^{1}D with H$_2$O vapour yielding two OH radicals, and ozonolysis is considered. The measured total OH reactivity (Whalley et al., 2016) which is representative of the sum of the concentration of all the individual OH sinks present multiplied by their bimolecular rate coefficients for reaction with OH is used as the denominator (E6).

The [OH]$_{PSS}$ time-series is overlaid with the OH observations in Figures 2 and 3 and, on the whole is able to predict the observed [OH] reasonably well, particularly during the south-westerly flows. The campaign median ratio of the rate of OH production to the turnover rate of OH (D_{OH}), equal to the product of the total OH reactivity and the observed [OH] concentration, is close to 1 throughout the day (Fig. 4) highlighting consistency between the OH, HO$_2$ and OH reactivity observations as well as the ancillary, co-located HONO (Lee et al., 2016) and NO observations (Lee et al., 2009). From late morning and throughout the afternoon, when NO concentrations dropped, the production rate of OH from HONO photolysis

becomes competitive with the rate of production of OH from the secondary reaction of HO_2 with NO. . During the easterly conditions experienced at the beginning of the IOP, $[OH]_{PSS}$ does under-predict the observed [OH] between 10 am – 6 pm (Fig. 2), however, suggesting that, if all the observed OH sources used in the PSS calculation are correct, there may be a missing OH source under these conditions (discussed further below). The small OH interference deriving from the photolysis of O_3 within the FAGE cell (determined through laboratory tests) is corrected for in all OH data presented. Interestingly, when the wind direction switched for a second time to an easterly flow, $[OH]_{PSS}$ reproduces the observed [OH] well (Fig. 2, lower panel).

A zero dimensional box model (MCM-BASE), which is run unconstrained to the radicals, but constrained to all other measured OH sources and constrained to the very detailed VOC observations (Table 3 provides the mean and maximum noontime concentration for all model constraints both under south westerly and easterly flows) performs much better than $[OH]_{PSS}$ during the first period of easterlies from late morning until late evening. However, under south-westerly conditions and also under the easterly conditions encountered during the second half of the campaign MCM-BASE over-predicts [OH] during the daytime by ~25% during the south-westerlies and by over a factor of 2 during the easterlies encountered at the end of the campaign. The box model also has a tendency to under-predict the observed [OH] during the morning rush-hour (from dawn – 10 am) throughout the IOP. Since the model is able to reproduce the observed OH reactivity well during the easterly flows (Whalley et al., 2016), an under-estimation of the total sink term for OH is not the cause of the daytime (10am to 6pm) discrepancy. Rather, as can be seen in Fig. 2 and Fig. 3, this model significantly over-predicts the observed $[HO_2]$ by close to a factor of 10 during the day under easterly conditions. The model over-estimates the total RO_2 concentration observed by close to a factor of two during the easterly flows but predicts RO_2i well in this airmass. It should be noted that the model RO_2 is simply the sum of all individual RO_2 species that the model predicts from the VOCs it is constrained to and no attempt is made to subtract the contribution of RO_2 species that RO_xLIF may have a low sensitivity to. This model-measurement RO_2 discrepancy could, therefore, indicate the presence of RO_2 species which do not readily convert to HO_2 in the RO_xLIF reactor in these easterly flows. Alternatively the modelled RO_2 over-estimate may either be due to the model over-estimating the sources of RO_2 or under estimating RO_2 sinks. Previous work (Whalley et al., 2016) highlighted that in general the model was able to capture the observed OH reactivity (k_{OH}) well during the easterly conditions encountered once the contribution to reactivity from mono-terpenes and the heavier-weight alkanes which derive from diesel emissions (Dunmore et al., 2015) was considered. This agreement between modelled and observed k_{OH} suggests that the production of RO_2 from the oxidation of VOCs by OH should be reasonably well captured by the model and suggests that the model-measurement disagreement during the easterly flow may derive from an under-estimation of the RO_2 sinks. During the south-westerly flows, the model is able to capture the observed $[RO_2]$ and $[RO_2i]$ well during the afternoon on most days. However, the model under predicts the observed $[RO_2]$ throughout the morning hours and into the early afternoon (Fig. 3a). Our previous work highlighted that this model slightly under-predicted the observed OH reactivity (by ~25%) during south-westerly flows (Whalley et al., 2016) and

indicates, therefore, that a RO$_2$ source (from the oxidation of VOCs by OH) may be missing from the model under these conditions.

Despite the factor of 5 increase in modelled [HO$_2$] as the air-mass arriving at the site switched from south-westerly to easterly (the [HO$_2$] increase is driven to a large extent by the increase in [HCHO] a major source of HO$_2$ under easterly flows), [OH] observed (and modelled) increased by only ~35% on average. This demonstrates that the increase in OH sources was almost entirely compensated for by an equivalent increase in OH sinks during these different flow regimes. The differences between [OH]$_{PSS}$ and [OH]$_{MCM\text{-}BASE}$ observed throughout the IOP reflects the impact of changing HO$_2$, the dominant OH source (see section 3.2) by an order of magnitude without changing the total OH sink term.

During 4 nights of the IOP, [RO$_2$] is predicted to be elevated, reaching concentrations of $>1\times10^{10}$ molecule cm^{-3} at 8 pm on 24th July. These high nighttime [RO$_2$] were not observed, to the magnitude predicted by the model, and other radical types (OH and HO$_2$) were not observed nor predicted to increase at the same time. These high modelled RO$_2$ excursions correspond to evenings when VOC concentrations were elevated and NO concentrations low and reflect periods of active nitrate chemistry in the model (see brown area, fig. 6). The RO$_x$LIF technique is likely insensitive to some NO$_3$-adduct alkene peroxy radicals. Only around 20% of the short-chain alkene derived NO$_3$-adduct peroxy radicals (e.g. those deriving from ethene and propene) are expected to convert to HO$_2$ in the reactor with the dominant reaction pathway (around 80%) instead leading to the formation of two aldehydes and NO$_2$ (according to the MCM). For the NO$_3$-adduct peroxy radical deriving from isoprene, however, the MCM assumes 100% yield of HO$_2$. The insensitivity of RO$_x$LIF to certain NO$_3$-adduct alkene peroxy radicals may explain the RO$_2$ model measurement discrepancy in the nighttime.

3.2 Model radical budget analysis

Figure 5 shows the main initiation, propagation and termination pathways in the model, and the hourly mean diel profiles of the modelled rates of primary radical initiation and termination are shown in Figure 6. Similar budget analyses have been conducted at other urban locations and may be compared and contrasted with the radical cycling here. During ClearfLo, the chain termination reaction of OH with NO$_2$, which leads to a net loss of radicals accounts for 24% of the modelled loss of OH between 6am – 9pm (21% for 11am-3pm if morning and evening rush-hours are excluded) (Whalley et al., 2016). For comparison, this reaction contributed 20% to the total modelled OH loss in Los-Angeles during CALNEX (Griffith et al., 2016), 19% in Mexico City during MCMA-2006 (Dusanter et al., 2009), and just 11% in Birmingham during PUMA during the summer (11am-3pm) (Emmerson et al., 2005b).

In terms of total radical destruction reactions, OH+NO$_2$ accounts for 32% (red area, Fig. 6, lower panel), with net (forward – backward) RO$_2$ + NO$_2$ to PAN species accounting for 35% (green area, Fig. 6, lower panel). As shown in Figure 6, the termination of RO$_x$ is dominated by loss of the OH radical (by reaction with NO$_2$) during the morning, whilst during the afternoon, radical termination is dominated by the loss of RO$_2$ species via PAN formation. In Birmingham, during the PUMA

campaign (Emmerson et al., 2005b) net PAN formation reactions contributed close to 50% of the total radical destruction pathways reflecting the high OVOC fraction of total VOCs present, particularly aldehydes, in Birmingham. The photolysis of HONO is the dominant primary radical source in London, accounting for 40% of the total radical initiation steps between 11am -3pm (Lee et al., 2016); the photolysis of formaldehyde to yield two HO_2 radicals contributes 20%, whilst $O(^1D)+H_2O$

5 contributes 12% and ozonolysis reactions, only 9%. HONO photolysis contributed a significant fraction to radical initiation in the MCMA-2006 and CALNEX studies also. In Birmingham the contribution of HONO photolysis as a primary radical source was likely under-estimated as HONO was not measured directly. In London, the model significantly under-estimated [HONO] if only gas-phase reactions were considered (Lee et al., 2016). Ozonolysis reactions were identified as the most important primary source of radicals in Birmingham, with these reactions accounting for 25% of the radical initiation, which is much

10 more significant than for London and highlights the very different VOC profile that exists in these two major UK cities. The PUMA campaign took place in Birmingham in the 2000 and so the difference in the VOC speciation may reflect, in part, the change in VOC emissions in the UK over the past decade. As shown by Figure 6, blue area, ozonolysis reactions form an increasingly significant fraction of the radical initiation reactions during the afternoon hours and, along with $VOC+NO_3$ reactions, accounts for all the nighttime radical initiation reactions. Formaldehyde acts as a significant source of HO_2 radicals

15 in London via photolysis and its reaction with OH. The latter, (OH to HO_2) propagation step (including OH+HCHO, but also OH+CO, OH+aromatics and OH+O_3) accounts for 27% of all the OH reactions in London. This OH to HO_2 propagation step, which is lower at other urban sites (19% and 20% during CALNEX and MCMA-2006 and 11% in Birmingham) contributes, in part, to the high modelled HO_2 concentration predicted for ClearfLo.

The relative importance of the individual formation, propagation and termination reactions under south westerly and easterly

20 flows remains similar. However, as highlighted by Fig. 7, the rate of many of the reactions are at least twice as fast under the easterly flows with HO_2+RO_2 and RO_2+RO_2 reactions approximately 6 and 8 times faster respectively and NO_3+VOC reactions close to 4 times faster.

3.3 Observed and modelled HO_x radical behaviour as a function of NO

25 As highlighted in Fig. 2 and 3, the degree of model-to-measured agreement varies depending on the chemical conditions encountered, which changed as a function of the wind direction and time of day. To gain further insight into chemical regimes under which model performance becomes compromised, the observed and modelled radical trends as a function of NO is considered and are shown in Fig. 8 and 9.

3.3.1 Low NO

30 This analysis highlights that under low [NO] conditions (< 1 ppbv) the median $[OH]_{MCM-BASE}$ and $[OH]_{obs}$ agree reasonably well (black and blue squares, Fig. 8, upper panel), whilst the $[OH]_{PSS}$ (orange squares) under-estimate the observations by

~35% (and up to a factor of 3 during the first easterlies). By expanding the number of bins representing the OH data at [NO] < 1 ppbv (Fig. 9) it is evident that both the MCM-BASE and PSS calculation under-estimate the observed OH at [NO]<0.5 ppbv, with the MCM-BASE agreeing with the observations between 0.5 – 1 ppbv [NO]. Beyond 1 ppbv [NO], [OH]$_{obs}$ and [OH]$_{PSS}$ are in good agreement.

5 In several other urban studies, during which a range of NO$_x$ conditions were encountered, a tendency to under-predict the observed [OH] at [NO] below 1 ppbv has been reported (Kanaya et al., 2007; Lu et al., 2012; Lu et al., 2013). As noted above in section 3.1, the differences in the MCM-BASE and PSS model predictions observed for ClearfLo at low [NO] derives from the large over-estimation of HO$_2$ by the box model. If the box model is missing a large peroxy radical sink (discussed further in section 4 below) and, as such, a model constrained to the observed HO$_2$ provides a better representation of the OH sources,

10 then, in agreement with the findings from Tokyo and China, an OH source important under low NO$_x$ conditions must be missing from the model mechanism for London. In both central Tokyo (Kanaya et al., 2007) and Beijing (Lu et al., 2013) an observed-to-modelled OH ratio of ~ 2 – 3 was found at 200 pptv NO. At [NO] 0.2 – 1 ppbv, the median [OH]$_{obs}$ to [OH]$_{PSS}$ ratio was ~1.5 for ClearfLo; the mean ratio was ~3 reflecting the larger difference between the observed OH and [OH]$_{PSS}$ during the first easterlies. Lu et al., (2013) considered an additional recycling mechanism of HO$_2$ to OH by an unknown species

15 and found that the rate of recycling required to reconcile the modelled and measured OH in Beijing was roughly half that required in during an earlier study conducted in the Pearl River Delta (Lu et al., 2012).

In contrast to the findings from these field observations made in China where [HO$_2$] modelled and observed were generally in reasonable agreement, the peroxy radical concentrations measured in London, particularly HO$_2$ concentrations, were greatly over-estimated by MCM-BASE under lower NO$_x$ conditions. It is interesting to note that HO$_2^*$ which comprises HO$_2$ and a

20 fraction of RO$_2$ radicals that rapidly decompose to HO$_2$ within low pressure FAGE cells (RO$_2i$) (Fuchs et al., 2011; Whalley et al., 2013) more closely follows the decrease in HO$_2$ predicted by the box model under the low NO conditions, than the interference-free HO$_2$ concentration that was observed (Fig. 8b). As shown in Fig. 8b, the HO$_2$ and HO$_2^*$ observations display the greatest deviation from each other at the lowest NO concentrations encountered and as NO concentrations increased the two measurements merged (i.e. HO$_2$ represented an increasing fraction of the HO$_2^*$ signal). The lowest [NO] tended to occur

25 during the daytime after the morning rush-hour and so considering the diurnal profile of RO$_2$ radicals (i.e. peak concentrations during the day, low concentrations during the night and early morning) this trend is perhaps expected. There was variability in the HO$_2$:HO$_2^*$ ratio day-to-day with a smaller ratio observed under easterly conditions compared to south-westerly conditions. The similarity in the HO$_2$ and HO$_2^*$ concentrations at high NO (Fig. 8b) demonstrates that the HO$_2$ artefact signal from RO$_2$ radicals is unlikely to contribute to any model measured discrepancies under high NO$_x$ conditions as discussed below. It is

30 possible that previous HO$_2$ measurements made at urban sites which did not correct for the RO$_2$ artefact (Fuchs et al., 2011; Whalley et al., 2013) may have masked a problem with model predictions of HO$_2$ under lower NO conditions. Recent radical observations made in Wangdu, a rural site in the North China Plain, however, which corrected HO$_2$ for possible RO$_2$ interferences, did not highlight any model deviation from measured HO$_2$ under low NO conditions (Tan et al., 2017). The

model over-estimation of HO$_2$ (and higher peroxy radicals) during ClearfLo, therefore, may be a reflection of the model's skill to predict radical propagation in the presence of the complex VOC mix which was observed in central London. The VOCs observed in London included a range of long-chain hydrocarbons deriving from diesel emissions as well as a range of monoterpene emissions from biogenic sources. This breakdown in model performance will be discussed further in section 4.

3.3.2 High NO

During ClearfLo, at [NO] > 15 ppbv, encountered primarily during the mornings, the modelled [OH]$_{MCM-BASE}$ underpredicted the observed [OH]. However, [OH]$_{PSS}$ was able to reproduce the OH measurements well (out to [NO] = 25 ppbv), as seen in Fig. 8. The under-prediction in OH by the MCM-BASE corresponds to an under-prediction in HO$_2$ between 15 – 30 ppbv NO. An under-prediction in HO$_2$ at elevated [NO] has been highlighted during a number of earlier urban studies (Martinez et al., 2003; Ren et al., 2013; Brune et al., 2016). Brune et al. (2016) measured HO$_2$ concentrations that were a factor of ten greater than those predicted when NO concentrations reached 10 ppbv during the CalNex study which took place in Bakerfield, US. During ClearfLo, the modelled and observed HO$_2$ were in good agreement under NO concentrations ranging from 7 – 15 ppbv, but beyond 15 ppbv the model did begin to under-estimate the observations by approximately a factor of 3. It should be noted that the number of radical observations made under these elevated [NO$_x$] were relatively few and, in fact at [NO] concentrations greater than 30 ppbv, the model and observed HO$_2$ converge once more (Fig. 8). At high NO$_x$, Brune and co-workers report a measured OH production rate (P_{OH}) (determined by summing the rates of production from all measured OH sources) which was about twice the measured OH turnover rate (determined from the product of the total OH reactivity and observed [OH]) highlighting an inconsistency between the OH, HO$_2$ and OH reactivity observations. In contrast to this, as demonstrated by the good agreement between the median observed OH production and OH loss rates during ClearfLo (Fig. 4), the [HO$_2$] observed at the highest NO is supported by the observed [OH] and OH reactivity.

The median modelled and measured total RO$_2$ and RO$_2$$i$ trend as a function of NO are shown in Fig. 10. The model predicts RO$_2$ well at [NO] < 1 ppbv; the over-prediction of total RO$_2$ during the first easterlies does not bias the overall median model trend which, instead largely reflects the good agreement between modelled and measured RO$_2$ under the dominating south-westerly conditions at low [NO]. In contrast to the reasonable agreement between modelled and observed HO$_2$ at high [NO], the model increasingly under-predicts the total RO$_2$ concentration (particularly RO$_2$$ni$) at [NO] beyond ~ 3 ppbv. As highlighted in Fig S3 in the SI, applying a correction to the RO$_2$ data to account for the possible decomposition of CH$_3$O$_2$NO$_2$ with the RO$_x$LIF flow reactor, leads to an improved agreement between the modelled and observations for RO$_2$ under high NO conditions although the extent to which CH$_3$O$_2$NO$_2$ decomposes within the flow reactor is highly uncertain. The photolysis of ClNO$_2$ to Cl atoms may provide an additional source of RO$_2$ radicals early in the morning as reported by Riedel et al. (2014). ClNO$_2$ was measured during the ClearfLo project (Bannan et al., 2015) and, although Cl atom chemistry can increase the modelled RO$_2$ concentrations in the morning when NO$_x$ levels are high, the predicted increase is modest, ~ 20%, and so cannot fully reconcile the model under-prediction in RO$_2$. For the more complex VOCs present (e.g. biogenics and the long-chain

alkanes) the rate of RO$_2$ propagation vs RO$_2$ termination may be faster than assumed in the model which would help to bring the model into better agreement with the observations.

4 Discussion

4.1 Possible explanations for the differences between observed and modelled peroxy radical concentrations at low NO

A number of possible explanations for the differences between the observed and modelled peroxy radical concentrations under the low NO conditions have been explored through a series of model scenarios (detailed below and also in the SI). The impact of [NO$_x$] deviations from a photo-stationary steady state in the real atmosphere as well as under-estimating the heterogeneous loss of HO$_2$ to aerosol surfaces are discussed in the SI and model runs highlighting the sensitivity of the modelled radical concentrations to these parameters are presented in Fig. S4. Enhancing the rate of HO$_2$ termination in the model, e.g. by enhancing the uptake probability of HO$_2$ to aerosols only improves the HO$_2$ modelled to measured agreement by a modest amount, and so, given the dominant reactions involving HO$_2$ are radical propagating, with the reaction of RO$_2$ + NO acting as the largest source of HO$_2$ and the reaction of HO$_2$ with NO (recycling OH) acting as the dominant HO$_2$ sink (Fig. 5), this raises the question whether the model discrepancy relates to uncertainties in the RO$_2$ oxidation chemistry and the cycling of RO$_2$ to HO$_2$. Of particular relevance are the reactions involving the complex RO$_2$ species deriving from VOCs emitted from diesel and biogenic sources.

Hydrocarbon autoxidation processes which are known to readily occur in the liquid phase (Bolland, 1949) were, until recently, thought to be unimportant in the gas-phase owing to the low probability of intermolecular H-atom abstraction. The low probability is due to the low concentration of hydrocarbons in the atmosphere and the competition between intra-molecular H-shift reactions (from a C-H to an R-O-O bond forming a peroxide) and bimolecular reactions of the RO$_2$ radical (e.g. with NO, HO$_2$ or RO$_2$). There is increasing evidence, however, that autoxidation processes are occurring in the atmosphere, which can quickly lower the volatility of VOCs and promote SOA formation. Laboratory studies have shown that monoterpenes, α-pinene and limonene, following initial attack by ozone or OH form highly oxidised RO$_2$ radicals within a few seconds via repeated H-shift from C-H to an R-O-O bond and subsequent O$_2$ additions (Crounse et al., 2011; Jokinen et al., 2014; Ehn et al., 2014; Berndt et al., 2016). Mass spectrometric signals relating to these highly oxidised RO$_2$ species have also been observed during field measurements (Jokinen et al., 2014). Autoxidation processes could be relevant during ClearfLo and omission of these processes in the model mechanism could account for some of the radical over-prediction observed under the lower NO conditions, particularly under easterly flow conditions when elevated concentrations of monoterpenes were observed. At high NO, bimolecular RO$_2$+NO reactions likely out-compete intramolecular processes. Importantly here, autoxidation steps which involve intramolecular H-atom abstraction from a C-H to an O-O bond and subsequent addition of O$_2$ to reform a more oxidised RO$_2$ radical do not generate HO$_2$. Jokinen et al., (2014) observed a high formation rate of organic nitrates (of the order of 30%)

when NO was added to experiments which would serve to further decrease RO_2 to HO_2 propagation. For ClearfLo conditions, a model run unconstrained to the mono-terpenes and the heavier-weight alkanes (MCM-VOC-STANDARD) under-estimated OH reactivity (Whalley et al., 2016) with the missing OH reactivity fraction largely reconciled by the model-generated intermediates which derive from alpha-pinene and limonene. If the current oxidation mechanism for these species is inaccurate, the reactivity attributed to these oxidation products could be wrong and instead may derive from other oxidised species. The missing reactivity in the MCM-VOC-STANDARD run can be included by adding a single OH to RO_2 conversion to the model equivalent to the missing reactivity (in s^{-1}) at each time stamp. To represent an autoxidation pathway, we convert OH to MCM species C6H5O2. This RO_2 species is formed via a minor phenol + OH channel. C6H5O2 does not readily convert to HO_2 by reaction with NO (due to the lack of available H on the alpha C) and, instead, following oxygen atom abstraction, C6H5O reacts with NO_2 to form a nitro-phenol, or reacts with ozone to reform C6H5O2; which reacts with further NO and so on. We do not consider the reactions of C6H5O2 to be representative of what is actually occurring, but rather choose this species to represent a mechanism by which the propagation of RO_2 to HO_2 is inhibited. Inclusion of OH→C6H5O2 leads to a ~30% decrease in modelled HO_2 (see pale blue vs black diel profiles in Fig. 11) and close to a 50% decrease in modelled HO_2 if the heterogeneous loss to aerosol is enhanced also by increasing the HO_2 uptake probability to aerosols from 0.1 to 1 (purple vs black diel profiles in Fig. 11). Including autoxidation in the model improves the agreement with the observations during the daytime for all radical species apart from the total RO_2 species observed during south westerly flows. As discussed in section 3.1, however, the model is, likely, missing VOCs under this air-mass regime (implied from the under-prediction of the observed k_{OH}) and this may contribute to the model under-prediction of RO_2. The under-prediction of RO_2i when an autoxidation step is included is due to the choice of OH→RO_2 conversion species (i.e. C6H5O2 is an RO_2 species that does not decompose to HO_2 in the presence of NO within a FAGE cell). The model under-prediction of RO_2i suggests that at least some of the RO_2 species that undergo autoxidation are species that would decompose to HO_2 within a FAGE cell.

The partitioning of larger, lower volatility OVOCs to the aerosol-phase may be another important step which is not included in the model. The partitioning of gases to the aerosol-phase will reduce RO_2 to HO_2 propagation and act as a net radical sink and omitting this process may further contribute to some of the discrepancy between observed radical concentrations and MCM-BASE predictions.

As depicted by the model radical flux (Fig. 5) roughly half (162×10^5 molecule $cm^{-3}s^{-1}$ of 314×10^5 molecule $cm^{-3}\,s^{-1}$ between 11am – 3pm) of the modelled RO_2 radicals that react with NO eventually form HO_2 (via an alkoxy radical, RO). If, however, RO_2 to HO_2 propagation is over-estimated by the model due to the uncertainties outline above, modelled HO_2 may become artificially high. A steady state $[HO_2]$ can be estimated (without the use of a model) by balancing the dominant HO_2 production and destruction reactions (first and second order loss processes) that occur:

$$k_{CO+OH}[CO][OH]+k_{HCHO+OH}[HCHO][OH]+2 \times j(HCHO_{radical\ channel})[HCHO]+(\alpha \times k_{RO_2+NO}[RO_2][NO])$$

$$= k_{HO_2+HO_2}[HO_2]^2 + k_{HO_2+NO}[NO][HO_2] + k_{HO_2+RO_2}[RO_2][HO_2] + k_{HO_2+O_3}[O_3][HO_2] + k_{Loss\ to\ Aerosols}[HO_2] \quad (7)$$

α is equal to the fraction of RO$_2$ radicals which propagate to HO$_2$ (which is roughly half in MCM-BASE).

Eqn. 16 can be rewritten as a quadratic equation for HO$_2$ and then solved for HO$_2$ to yield the following solution:

$$[HO_2] = \frac{-b + \sqrt{(b^2 - 4ac)}}{2a} \quad (8)$$

where

$$a = 2 \times k_{HO_2+HO_2} \quad (9)$$

$$b = k_{HO_2+NO}[NO] + k_{HO_2+RO_2}[RO_2] + k_{HO_2+O_3}[O_3] + k_{Loss\ to\ Aerosols} \quad (10)$$

$$c = k_{CO+OH}[CO][OH] + k_{HCHO+OH}[HCHO][OH] + 2 \times j(HCHO_{radical\ channel})[HCHO] + (\alpha \times k_{RO_2+NO}[RO_2][NO])$$

$$(11)$$

Using the observed RO$_2$ and OH concentrations in equations E8 – E11 above to calculate [HO$_2$], generally good agreement between HO$_2$ observed and HO$_2$ calculated can be achieved if α equal to 0.15 is assumed as shown in Figure 12. Using an α = 0.15, leads to a model under-prediction of HO$_2$ for the higher NO$_x$ conditions experienced in the early morning, however. This may indicate that α is dependent on NO concentrations and likely the VOC speciation too. Furthermore, the value for α is sensitive to the rate coefficient, k_{RO_2+NO} used with the [HO$_2$] in Fig. 11 calculated using $k_{RO_2+NO} = k_{CH_3O_2+NO}$ (= 7.7×10^{-12} cm^3 molecule^{-1}s^{-1} at 298K). If some of the RO$_2$ species contributing to the total RO$_2$ measured react faster with NO (as is the case for CH$_3$CO.O$_2$ radicals, k_{RO_2+NO}= 2×10^{-11} cm^3 molecule^{-1}s^{-1} at 298K), α would become <0.15. This low fraction of RO$_2$ to HO$_2$ conversion (if this is the cause for the observed and modelled discrepancy) compared to α~0.5 in MCM-BASE highlights a significant misunderstanding in the oxidation chemistry mechanism of the larger more complex VOCs. This misunderstanding likely becomes increasingly important in low NO, high VOC environments such as forests.

4.2 Impact of the model uncertainties on predictions of *in situ* ozone production

Poor representation of the observed peroxy radical concentration leads to significantly more ozone production predicted by the model than is calculated from the observed concentrations under low NO conditions (Fig. 13) using E1 (which is repeated below for clarity). Conversely, significantly less ozone production is predicted by the modelled peroxy radicals than by the observed peroxy radicals as [NO] increases.

$$P(O_3) = (k_{HO_2+NO}[HO_2][NO] + k_{RO_2+NO}[RO_2][NO]) - (k_{OH+NO_2+M}[OH][NO_2][M] + k_{RO_2+NO_2+M}[RO_2][NO_2][M])$$

$$(1)$$

As highlighted in section 3.3, the model's failure to predict the observed HO_2 radical concentrations is most evident under low NO_x conditions, typically experienced during the afternoon hours and particularly during easterly flows. At this time the observed ozone concentrations peaked (Fig. 13) due to reduced destruction by titration with NO. At NO concentrations <3 ppbv, the ozone production rate determined from the modelled peroxy radical concentrations remains relatively constant at ~3 ppbv hr^{-1} until very low levels of NO. $P(O_3)$ calculated with the observed peroxy radical, however, decreases to ~1 ppbv hr^{-1}. Under higher NO_x conditions, [NO]>3 ppbv, the ozone production rate determined from the modelled peroxy radical concentrations is, up to, an order of magnitude lower than the ozone production rate calculated from the observations (which at the highest [NO] reaches ~30 ppbv hr^{-1}). The calculation of ozone production from many earlier urban studies often relied on an inferred RO_2 concentration, estimated from the measured [HO_2] and assumed value of RO_2:HO_2, as measurements of total RO_2 were not available (e.g. (Ren et al., 2013; Brune et al., 2016)). In these studies, under high NO conditions, the $P(O_3)$ calculated from the observed HO_2 (and inferred RO_2) was significantly greater than $P(O_3)$ calculated using the modelled HO_2 and RO_2, reflecting the model under-estimation of HO_2 at high NO reported from these studies. In the recent Wangdu study conducted in China, Tan et al., (2017), using observed RO_2, demonstrated that models may under-predict ozone production at high NO due to an underestimation of the RO_2 radical concentration rather than under-estimation of HO_2. In the Wangdu study modelled and measured HO_2 were in good agreement at high NO. From the rate of ozone production calculated from the modelled and measured peroxy radicals for ClearfLo, we would draw similar conclusions as drawn by Tan and co-workers, i.e. that there is missing RO_2 at high NO, if the correction for decomposition of $CH_3O_2NO_2$ was not applicable. Although there are some uncertainties surrounding the magnitude of $CH_3O_2NO_2$ decomposition in the RO_xLIF cell (which is experimentally difficult to determine), in agreement with Tan et al. we find no evidence from the ClearfLo HO_2 dataset that there is a significant model bias for HO_2 which influences the model predicted $P(O_3)$ under the elevated NO conditions encountered.

The discrepancy between model and observations at low NO may arise from the model uncertainties in the treatment of the oxidation and removal of the complex VOC species observed as discussed above. The oxidation of these complex species tend not to be included in air quality models used to predict ozone and other secondary pollutants. The MCM, however, is used as the benchmark mechanism against which simpler mechanisms used within air quality models are tested (Malkin et al., 2016) and so the chemistry of these complex VOCs present in the urban atmosphere and the impact they have on peroxy radical concentrations needs to be adequately resolved.

5 Conclusions

Measurement and model comparisons of OH, HO_2, RO_2i and total RO_2, have displayed varying levels of agreement as a function of NO_x. Under higher NO_x conditions the box model increasingly under-predicted total $[RO_2]$ and, as a consequence, ozone production derived from the predicted peroxy radicals is up to an order of magnitude lower than from the observed peroxy radicals.

A large uncertainty in peroxy radical cycling, $RO_2 \rightarrow HO_2$, has been identified under lower NO conditions experienced during the daytime. We hypothesise that uncertainties in the degradation mechanism of RO_2 deriving form complex biogenic and diesel related VOC, species which were particularly elevated and dominated the OH reactivity under easterly flows when the model measurement discrepancy was largest, may account for the model measurement disagreement. Autoxidation processes now known to play a role in the chemical oxidation of mono-terpenes in the gas-phase, and which can enhance SOA formation, may serve to reduce the rate of RO_2 to HO_2 propagation under lower NO conditions. Omission of this oxidation process from the model mechanism leads to more ozone production predicted using modelled peroxy radical concentrations versus those measured, at a time when ozone destruction (by NO titration) is slow. Although air quality models do not typically consider these VOC types and tend to run with simplified chemistry schemes, the MCM is viewed as a benchmark mechanism against which these simpler chemistry schemes may be tested. Hence, these uncertainties in the mechanism identified here need to be critically assessed through further laboratory and field measurements.

Acknowledgements

The work was supported by the National Environment Research Council (NERC) through grant NE/H003193/1. We are also grateful to the National Centre for Atmospheric Science, which is funded by NERC, for ongoing support. We would like to thank all participants of ClearfLo for their help in supporting these measurements.

References

Barlow, J. F., Halios, C. H., Lane, S. E., and Wood, C. R.: Observations of urban boundary layer structure during a strong urban heat island event, Environmental fluid mechanisms, 15, 373-398, 2015.

Berndt, T., Richters, S., Jokinen, T., Hyttinen, N., Kurten, T., Otkjaer, R. V., Kjaergaard, H. G., Stratmann, F., Herrmann, H., Sipila, M., Kulmala, M., and Ehn, M.: Hydroxyl radical-induced formation of highly oxidized organic compounds, Nat Commun, 7, Artn 1367710.1038/Ncomms13677, 2016.

Bigi, A., and Harrison, R. M.: Analysis of the air pollution climate at a central urban background site, Atmos Environ, 44, 2004-2012, 10.1016/j.atmosenv.2010.02.028, 2010.

Bohn, B., Heard, D. E., Mihalopoulos, N., Plass-Dulmer, C., Schmitt, R., and Whalley, L. K.: Characterisation and improvement of j((OD)-D-1) filter radiometers, Atmos Meas Tech, 9, 3455-3466, 10.5194/amt-9-3455-2016, 2016.

Bohnenstengel, S. I., Belcher, S. E., Aiken, A., Allan, J. D., Allen, G., Bacak, A., Bannan, T. J., Barlow, J. F., Beddows, D. C. S., Bloss, W. J., Booth, A. M., Chemel, C., Coceal, O., Di Marco, C. F., Dubey, M. K., Faloon, K. H., Fleming, Z. L., Furger, M., Gietl, J. K., Graves, R. R., Green, D. C., Grimmond, C. S. B., Halios, C. H., Hamilton, J. F., Harrison, R. M., Heal, M. R., Heard, D. E., Helfter, C., Herndon, S. C., Holmes, R. E., Hopkins, J. R., Jones, A. M., Kelly, F. J., Kotthaus, S., Langford, B., Lee, J. D., Leigh, R. J., Lewis, A. C., Lidster, R. T., Lopez-Hilfiker, F. D., McQuaid, J. B., Mohr, C., Monks, P. S., Nemitz, E., Ng, N. L., Percival, C. J., Prevot, A. S. H., Ricketts, H. M. A., Sokhi, R., Stone, D., Thornton, J. A., Tremper, A. H., Valach, A. C., Visser, S., Whalley, L. K., Williams, L. R., Xu, L., Young, D. E., and Zotter, P.: Meteorology, Air Quality, and Health in London the Clearflo Project, B Am Meteorol Soc, 96, 779-804, 10.1175/Bams-D-12-00245.1, 2015.

Bolland, J. L.: Kinetics of olefin oxidation, Quarterly Reviews, Chemical Society, 3, 1-21, 1949.

Brune, W. H., Baier, B. C., Thomas, J., Ren, X., Cohen, R. C., Pusede, S. E., Browne, E. C., Goldstein, A. H., Gentner, D. R., Keutsch, F. N., Thornton, J. A., Harrold, S., Lopez-Hilfiker, F. D., and Wennberg, P. O.: Ozone production chemistry in the presence of urban plumes, Faraday Discuss, 189, 169-189, 10.1039/c5fd00204d, 2016.

Chen, S. A., Ren, X. R., Mao, J. Q., Chen, Z., Brune, W. H., Lefer, B., Rappengluck, B., Flynn, J., Olson, J., and Crawford, J. H.: A comparison of chemical mechanisms based on TRAMP-2006 field data, Atmos Environ, 44, 4116-4125, 10.1016/j.atmosenv.2009.05.027, 2010.

Commane, R., Floquet, C. F. A., Ingham, T., Stone, D., Evans, M. J., and Heard, D. E.: Observations of OH and HO_2 radicals over West Africa, Atmospheric Chemistry and Physics, 10, 8783-8801, 10.5194/acp-10-8783-2010, 2010.

Crounse, J. D., Paulot, F., Kjaergaard, H. G., and Wennberg, P. O.: Peroxy radical isomerization in the oxidation of isoprene, Phys Chem Chem Phys, 13, 13607-13613, 10.1039/c1cp21330j, 2011.

Dunmore, R. E., Hopkins, J. R., Lidster, R. T., Lee, J. D., Evans, M. J., Rickard, A. R., Lewis, A. C., and Hamilton, J. F.: Diesel-related hydrocarbons can dominate gas phase reactive carbon in megacities, Atmos Chem Phys, 15, 9983-9996, 10.5194/acp-15-9983-2015, 2015.

Dusanter, S., Vimal, D., Stevens, P. S., Volkamer, R., Molina, L. T., Baker, A., Meinardi, S., Blake, D., Sheehy, P., Merten, A., Zhang, R., Zheng, J., Fortner, E. C., Junkermann, W., Dubey, M., Rahn, T., Eichinger, B., Lewandowski, P., Prueger, J., and Holder, H.: Measurements of OH and HO_2 concentrations during the MCMA-2006 field campaign - Part 2: Model comparison and radical budget, Atmos Chem Phys, 9, 6655-6675, 2009.

5 Ehn, M., Thornton, J. A., Kleist, E., Sipila, M., Junninen, H., Pullinen, I., Springer, M., Rubach, F., Tillmann, R., Lee, B., Lopez-Hilfiker, F., Andres, S., Acir, I. H., Rissanen, M., Jokinen, T., Schobesberger, S., Kangasluoma, J., Kontkanen, J., Nieminen, T., Kurten, T., Nielsen, L. B., Jorgensen, S., Kjaergaard, H. G., Canagaratna, M., Dal Maso, M., Berndt, T., Petaja, T., Wahner, A., Kerminen, V. M., Kulmala, M., Worsnop, D. R., Wildt, J., and Mentel, T. F.: A large source of low-volatility secondary organic aerosol, Nature, 506, 476-+, 10.1038/nature13032, 2014.

10 Elshorbany, Y. F., Kleffmann, J., Hofzumahaus, A., Kurtenbach, R., Wiesen, P., Brauers, T., Bohn, B., Dorn, H. P., Fuchs, H., Holland, F., Rohrer, F., Tillmann, R., Wegener, R., Wahner, A., Kanaya, Y., Yoshino, A., Nishida, S., Kajii, Y., Martinez, M., Kubistin, D., Harder, H., Lelieveld, J., Elste, T., Plass-Dulmer, C., Stange, G., Berresheim, H., and Schurath, U.: HOx budgets during HOxComp: A case study of HOx chemistry under NOx-limited conditions, J Geophys Res-Atmos, 117, Artn D03307, 10.1029/2011jd017008, 2012.

15 Emmerson, K. M., Carslaw, N., Carpenter, L. J., Heard, D. E., Lee, J. D., and Pilling, M. J.: Urban atmospheric chemistry during the PUMA campaign 1: Comparison of modelled OH and HO_2 concentrations with measurements, J Atmos Chem, 52, 143-164, 10.1007/s10874-005-1322-3, 2005a.

Emmerson, K. M., Carslaw, N., and Pilling, M. J.: Urban atmospheric chemistry during the PUMA campaign 2: Radical budgets for OH, HO_2 and RO_2, J Atmos Chem, 52, 165-183, 10.1007/s10874-005-1323-2, 2005b.

20 Emmerson, K. M., Carslaw, N., Carslaw, D. C., Lee, J. D., McFiggans, G., Bloss, W. J., Gravestock, T., Heard, D. E., Hopkins, J., Ingham, T., Pilling, M. J., Smith, S. C., Jacob, M., and Monks, P. S.: Free radical modelling studies during the UK TORCH Campaign in Summer 2003, Atmos Chem Phys, 7, 167-181, 2007.

England, P. H.: Estimating local mortality burdens associated with particulate air pollution, 2014.

Fuchs, H., Holland, F., and Hofzumahaus, A.: Measurement of tropospheric RO2 and HO2 radicals by a laser-induced

25 fluorescence instrument, Rev Sci Instrum, 79, Artn 084104, 10.1063/1.2968712, 2008.

Fuchs, H., Bohn, B., Hofzumahaus, A., Holland, F., Lu, K. D., Nehr, S., Rohrer, F., and Wahner, A.: Detection of HO2 by laser-induced fluorescence: calibration and interferences from RO_2 radicals, Atmos Meas Tech, 4, 1209-1225, 10.5194/amt-4-1209-2011, 2011.

Fuchs, H., Hofzumahaus, A., Rohrer, F., Bohn, B., Brauers, T., Dorn, H. P., Haseler, R., Holland, F., Kaminski, M., Li, X.,

30 Lu, K., Nehr, S., Tillmann, R., Wegener, R., and Wahner, A.: Experimental evidence for efficient hydroxyl radical regeneration in isoprene oxidation, Nat Geosci, 6, 1023-1026, 10.1038/NGEO1964, 2013.

Fuchs, H., Tan, Z. F., Hofzumahaus, A., Broch, S., Dorn, H. P., Holland, F., Kunstler, C., Gomm, S., Rohrer, F., Schrade, S., Tillmann, R., and Wahner, A.: Investigation of potential interferences in the detection of atmospheric ROx radicals by laser-induced fluorescence under dark conditions, Atmos Meas Tech, 9, 1431-1447, 10.5194/amt-9-1431-2016, 2016.

Fuchs, H., Tan, Z. F., Lu, K. D., Bohn, B., Broch, S., Brown, S. S., Dong, H. B., Gomm, S., Haseler, R., He, L. Y., Hofzumahaus, A., Holland, F., Li, X., Liu, Y., Lu, S. H., Min, K. E., Rohrer, F., Shao, M., Wang, B. L., Wang, M., Wu, Y. S., Zeng, L. M., Zhang, Y. S., Wahner, A., and Zhang, Y. H.: OH reactivity at a rural site (Wangdu) in the North China Plain: contributions from OH reactants and experimental OH budget, Atmos Chem Phys, 17, 645-661, 10.5194/acp-17-645-2017, 2017.

George, L. A., Hard, T. M., and O'Brien, R. J.: Measurement of free radicals OH and HO_2 in Los Angeles smog, J Geophys Res-Atmos, 104, 11643-11655, Doi 10.1029/1998jd100113, 1999.

Gerbig, C., Schmitgen, S., Kley, D., Volz-Thomas, A., Dewey, K., and Haaks, D.: An improved fast-response vacuum-UV resonance fluorescence CO instrument, J Geophys Res-Atmos, 104, 1699-1704, Doi 10.1029/1998jd100031, 1999.

Griffith, S. M., Hansen, R. F., Dusanter, S., Michoud, V., Gilman, J. B., Kuster, W. C., Veres, P. R., Graus, M., de Gouw, J. A., Roberts, J., Young, C., Washenfelder, R., Brown, S. S., Thalman, R., Waxman, E., Volkamer, R., Tsai, C., Stutz, J., Flynn, J. H., Grossberg, N., Lefer, B., Alvarez, S. L., Rappenglueck, B., Mielke, L. H., Osthoff, H. D., and Stevens, P. S.: Measurements of hydroxyl and hydroperoxy radicals during CalNex-LA: Model comparisons and radical budgets, J Geophys Res-Atmos, 121, 4211-4232, 10.1002/2015JD024358, 2016.

Hayman, G. D.: Effect of pollution control on UV exposure, Oxfordshire, UK, 1997.

Heland, J., Kleffmann, J., Kurtenbach, R., and Wiesen, P.: A new instrument to measure gaseous nitrous acid (HONO) in the atmosphere, Environ Sci Technol, 35, 3207-3212, Doi 10.1021/Es000303t, 2001.

Hopkins, J. R., Lewis, A. C., and Read, K. A.: A two-column method for long-term monitoring of non-methane hydrocarbons (NMHCs) and oxygenated volatile organic compounds (o-VOCs), J Environ Monitor, 5, 8-13, 10.1039/b202798d, 2003.

Jenkin, M. E., Wyche, K. P., Evans, C. J., Carr, T., Monks, P. S., Alfarra, M. R., Barley, M. H., McFiggans, G. B., Young, J. C., and Rickard, A. R.: Development and chamber evaluation of the MCM v3.2 degradation scheme for beta-caryophyllene, Atmos Chem Phys, 12, 5275-5308, 10.5194/acp-12-5275-2012, 2012.

Jerrett, M., Burnett, R. T., Pope, C. A., Ito, K., Thurston, G., Krewski, D., Shi, Y. L., Calle, E., and Thun, M.: Long-Term Ozone Exposure and Mortality., New Engl J Med, 360, 1085-1095, Doi 10.1056/Nejmoa0803894, 2009.

Jokinen, T., Sipila, M., Richters, S., Kerminen, V. M., Paasonen, P., Stratmann, F., Worsnop, D., Kulmala, M., Ehn, M., Herrmann, H., and Berndt, T.: Rapid Autoxidation Forms Highly Oxidized RO_2 Radicals in the Atmosphere, Angew Chem Int Edit, 53, 14596-14600, 10.1002/anie.201408566, 2014.

Kanaya, Y., Cao, R. Q., Akimoto, H., Fukuda, M., Komazaki, Y., Yokouchi, Y., Koike, M., Tanimoto, H., Takegawa, N., and Kondo, Y.: Urban photochemistry in central Tokyo: 1. Observed and modeled OH and HO_2 radical concentrations during the winter and summer of 2004, J Geophys Res-Atmos, 112, Artn D21312, 10.1029/2007jd008670, 2007.

Kleffmann, J.: Daytime sources of nitrous acid (HONO) in the atmospheric boundary layer, Chemphyschem, 8, 1137-1144, 10.1002/cphc.200700016, 2007.

Konrad, S., Schmitz, T., Buers, H. J., Houben, N., Mannschreck, K., Mihelcic, D., Musgen, P., Patz, H. W., Holland, F., Hofzumahaus, A., Schafer, H. J., Schroder, S., Volz-Thomas, A., Bachmann, K., Schlomski, S., Moortgat, G., and Grossmann, D.: Hydrocarbon measurements at Pabstthum during the BERLIOZ campaign and modeling of free radicals, J Geophys Res-Atmos, 108, Artn 8251, 10.1029/2001jd000866, 2003.

5   Lee, J. D., Moller, S. J., Read, K. A., Lewis, A. C., Mendes, L., and Carpenter, L. J.: Year-round measurements of nitrogen oxides and ozone in the tropical North Atlantic marine boundary layer, J Geophys Res-Atmos, 114, Artn D21302, 10.1029/2009jd011878, 2009.

Lee, J. D., Whalley, L. K., Heard, D. E., Stone, D., Dunmore, R. E., Hamilton, J. F., Young, D. E., Allan, J. D., Laufs, S., and Kleffmann, J.: Detailed budget analysis of HONO in central London reveals a missing daytime source, Atmos Chem
10   Phys, 16, 2747-2764, 10.5194/acp-16-2747-2016, 2016.

Lidster, R. T., Hamilton, J. F., Lee, J. D., Lewis, A. C., Hopkins, J. R., Punjabi, S., Rickard, A. R., and Young, J. C.: The impact of monoaromatic hydrocarbons on OH reactivity in the coastal UK boundary layer and free troposphere, Atmos Chem Phys, 14, 6677-6693, 10.5194/acp-14-6677-2014, 2014.

Lu, K. D., Rohrer, F., Holland, F., Fuchs, H., Bohn, B., Brauers, T., Chang, C. C., Haseler, R., Hu, M., Kita, K., Kondo, Y.,
15   Li, X., Lou, S. R., Nehr, S., Shao, M., Zeng, L. M., Wahner, A., Zhang, Y. H., and Hofzumahaus, A.: Observation and modelling of OH and HO_2 concentrations in the Pearl River Delta 2006: a missing OH source in a VOC rich atmosphere, Atmos Chem Phys, 12, 1541-1569, 10.5194/acp-12-1541-2012, 2012.

Lu, K. D., Hofzumahaus, A., Holland, F., Bohn, B., Brauers, T., Fuchs, H., Hu, M., Haseler, R., Kita, K., Kondo, Y., Li, X., Lou, S. R., Oebel, A., Shao, M., Zeng, L. M., Wahner, A., Zhu, T., Zhang, Y. H., and Rohrer, F.: Missing OH source in a
20   suburban environment near Beijing: observed and modelled OH and HO2 concentrations in summer 2006, Atmos Chem Phys, 13, 1057-1080, 10.5194/acp-13-1057-2013, 2013.

Mao, J., Ren, X., Zhang, L., Van Duin, D. M., Cohen, R. C., Park, J. H., Goldstein, A. H., Paulot, F., Beaver, M. R., Crounse, J. D., Wennberg, P. O., DiGangi, J. P., Henry, S. B., Keutsch, F. N., Park, C., Schade, G. W., Wolfe, G. M., Thornton, J. A., and Brune, W. H.: Insights into hydroxyl measurements and atmospheric oxidation in a California forest,
25   Atmos Chem Phys, 12, 8009-8020, 10.5194/acp-12-8009-2012, 2012.

Martinez, M., Harder, H., Kovacs, T. A., Simpas, J. B., Bassis, J., Lesher, R., Brune, W. H., Frost, G. J., Williams, E. J., Stroud, C. A., Jobson, B. T., Roberts, J. M., Hall, S. R., Shetter, R. E., Wert, B., Fried, A., Alicke, B., Stutz, J., Young, V. L., White, A. B., and Zamora, R. J.: OH and HO2 concentrations, sources, and loss rates during the Southern Oxidants Study in Nashville, Tennessee, summer 1999, J Geophys Res-Atmos, 108, Artn 4617, 10.1029/2003jd003551, 2003.

30   Michoud, V., Kukui, A., Camredon, M., Colomb, A., Borbon, A., Miet, K., Aumont, B., Beekmann, M., Durand-Jolibois, R., Perrier, S., Zapf, P., Siour, G., Ait-Helal, W., Locoge, N., Sauvage, S., Afif, C., Gros, V., Furger, M., Ancellet, G., and Doussin, J. F.: Radical budget analysis in a suburban European site during the MEGAPOLI summer field campaign, Atmos Chem Phys, 12, 11951-11974, 10.5194/acp-12-11951-2012, 2012.

Novelli, A., Hens, K., Ernest, C. T., Kubistin, D., Regelin, E., Elste, T., Plass-Dulmer, C., Martinez, M., Lelieveld, J., and Harder, H.: Characterisation of an inlet pre-injector laser-induced fluorescence instrument for the measurement of atmospheric hydroxyl radicals, Atmos Meas Tech, 7, 3413-3430, 10.5194/amt-7-3413-2014, 2014.

Peters, T. M., and Leith, D.: Concentration measurement and counting efficiency of the aerodynamic particle sizer 3321, J Aerosol Sci, 34, 627-634, 10.1016/S0021-8502(03)00030-2, 2003.

Ravishankara, A. R.: Heterogeneous and multiphase chemistry in the troposphere, Science 276, 1058-1065, 1997.

Ren, X. R., Harder, H., Martinez, M., Lesher, R. L., Oliger, A., Simpas, J. B., Brune, W. H., Schwab, J. J., Demerjian, K. L., He, Y., Zhou, X. L., and Gao, H. G.: OH and HO2 chemistry in the urban atmosphere of New York City, Atmos Environ, 37, 3639-3651, 10.1016/S1352-2310(03)00459-X, 2003.

Ren, X. R., van Duin, D., Cazorla, M., Chen, S., Mao, J. Q., Zhang, L., Brune, W. H., Flynn, J. H., Grossberg, N., Lefer, B. L., Rappengluck, B., Wong, K. W., Tsai, C., Stutz, J., Dibb, J. E., Jobson, B. T., Luke, W. T., and Kelley, P.: Atmospheric oxidation chemistry and ozone production: Results from SHARP 2009 in Houston, Texas, J Geophys Res-Atmos, 118, 5770-5780, 10.1002/jgrd.50342, 2013.

Salmon, R. A., Bauguitte, S. J. B., Bloss, W., Hutterli, M. A., Jones, A. E., Read, K., and Wolff, E. W.: Measurement and interpretation of gas phase formaldehyde concentrations obtained during the CHABLIS campaign in coastal Antarctica, Atmos Chem Phys, 8, 4085-4093, 10.5194/acp-8-4085-2008, 2008.

Sheehy, P. M., Volkamer, R., Molina, L. T., and Molina, M. J.: Oxidative capacity of the Mexico City atmosphere - Part 2: A ROx radical cycling perspective, Atmos Chem Phys, 10, 6993-7008, 10.5194/acp-10-6993-2010, 2010.

Shirley, T. R., Brune, W. H., Ren, X., Mao, J., Lesher, R., Cardenas, B., Volkamer, R., Molina, L. T., Molina, M. J., Lamb, B., Velasco, E., Jobson, T., and Alexander, M.: Atmospheric oxidation in the Mexico City Metropolitan Area (MCMA) during April 2003, Atmos Chem Phys, 6, 2753-2765, 2006.

Stone, D., Whalley, L. K., and Heard, D. E.: Tropospheric OH and HO2 radicals: field measurements and model comparisons, Chem Soc Rev, 41, 6348-6404, 10.1039/c2cs35140d, 2012.

Stone, D., Whalley, L. K., Ingham, T., Edwards, P. M., Cryer, D. R., Brumby, C. A., Seakins, P. W., and Heard, D. E.: Measurement of OH reactivity by laser flash photolysis coupled with laser-induced fluorescence spectroscopy, Atmos Meas Tech, 9, 2827-2844, 10.5194/amt-9-2827-2016, 2016.

Tan, Z., Fuchs, H., Lu, K., Bohn, B., Broch, S., Dong, H., Gomm, S., Haseler, R., He, L., Hofzumahaus, A., Holland, F., Li, X., Liu, Y., Lu, S., Rohrer, F., Shao, M., Wang, B., Wang, M., Wu, Y., Zeng, L. M., Zhang, Y., Wahner, A., and Zhang, Y.: Radical chemistry at a rural site (Wangdu) in the North China Plain: Observation and model calculations of OH, HO_2 and RO_2 radicals, Atmos Chem Phys, 17, 663-690, 2017.

Thurston, G. D., Lippmann, M., Scott, M. B., and Fine, J. M.: Summertime haze air pollution and children with asthma, Am J Resp Crit Care, 155, 654-660, 1997.

Whalley, L. K., Lewis, A. C., McQuaid, J. B., Purvis, R. M., Lee, J. D., Stemmler, K., Zellweger, C., and Ridgeon, P.: Two high-speed, portable GC systems designed for the measurement of non-methane hydrocarbons and PAN: Results from the Jungfraujoch High Altitude Observatory, J Environ Monitor, 6, 234-241, 10.1039/b310022g, 2004.

Whalley, L. K., Furneaux, K. L., Goddard, A., Lee, J. D., Mahajan, A., Oetjen, H., Read, K. A., Kaaden, N., Carpenter, L. J., Lewis, A. C., Plane, J. M. C., Saltzman, E. S., Wiedensohler, A., and Heard, D. E.: The chemistry of OH and HO2 radicals in the boundary layer over the tropical Atlantic Ocean, Atmos Chem Phys, 10, 1555-1576, 10.5194/acp-10-1555-2010, 2010.

Whalley, L. K., Blitz, M. A., Desservettaz, M., Seakins, P. W., and Heard, D. E.: Reporting the sensitivity of laser-induced fluorescence instruments used for HO2 detection to an interference from RO_2 radicals and introducing a novel approach that enables HO2 and certain RO2 types to be selectively measured, Atmos Meas Tech, 6, 3425-3440, 10.5194/amt-6-3425-2013, 2013.

Whalley, L. K., Stone, D., Bandy, B., Dunmore, R., Hamilton, J. F., Hopkins, J., Lee, J. D., Lewis, A. C., and Heard, D. E.: Atmospheric OH reactivity in central London: observations, model predictions and estimates of in situ ozone production, Atmos Chem Phys, 16, 2109-2122, 10.5194/acp-16-2109-2016, 2016.

Woodward-Massey, R., Slater, E., Ye, C., Seakins, P. W., Whalley, L. K., and Heard, D. E.: Assessment of interferences during field measurements of OH using a laser-induced fluorescence instrument equipped with a scavenger injector, EGU, Vienna, Austria, 2017.
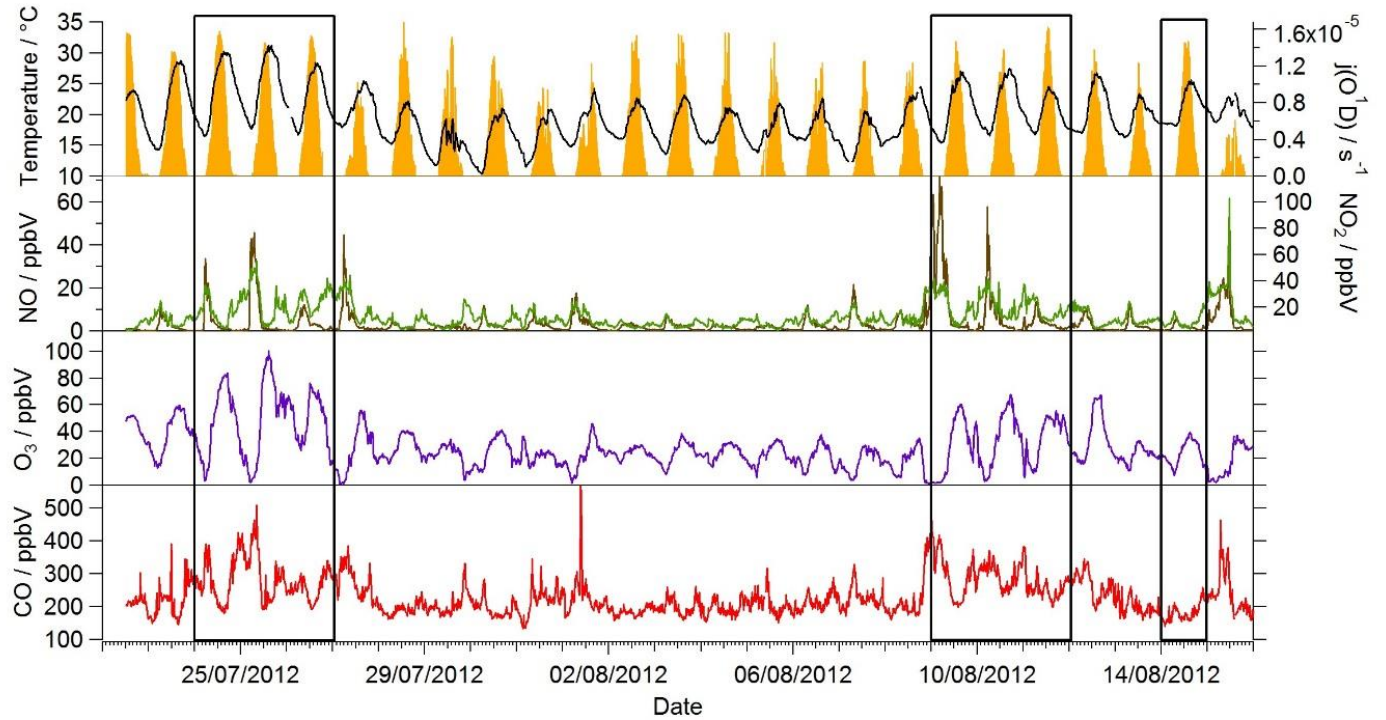
Figure 1: Observed temperature (black line), j(O¹D) (yellow area), NO (brown line), NO₂ (green line), O₃ (purple line) and CO (red line) mixing ratios during the summer ClearfLo IOP. Data time resolution is 15 minutes. Periods of Easterly flow are highlighted inside the black boxes.
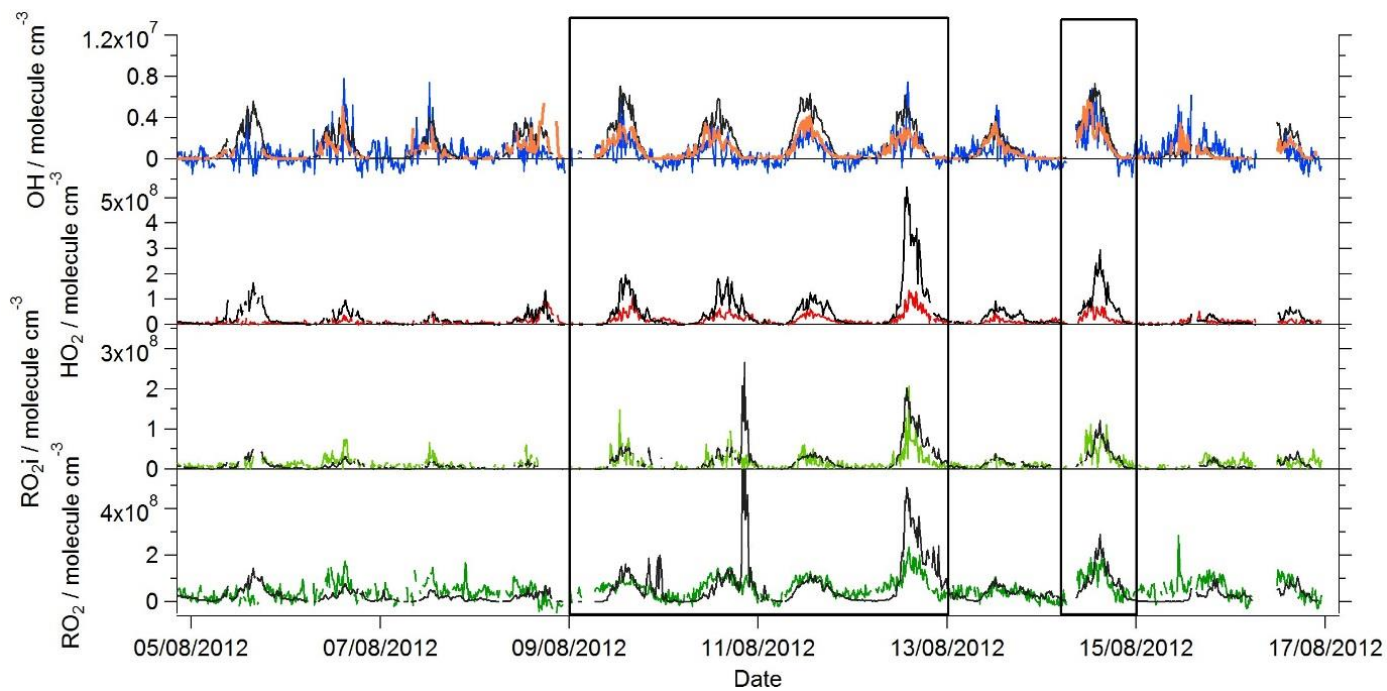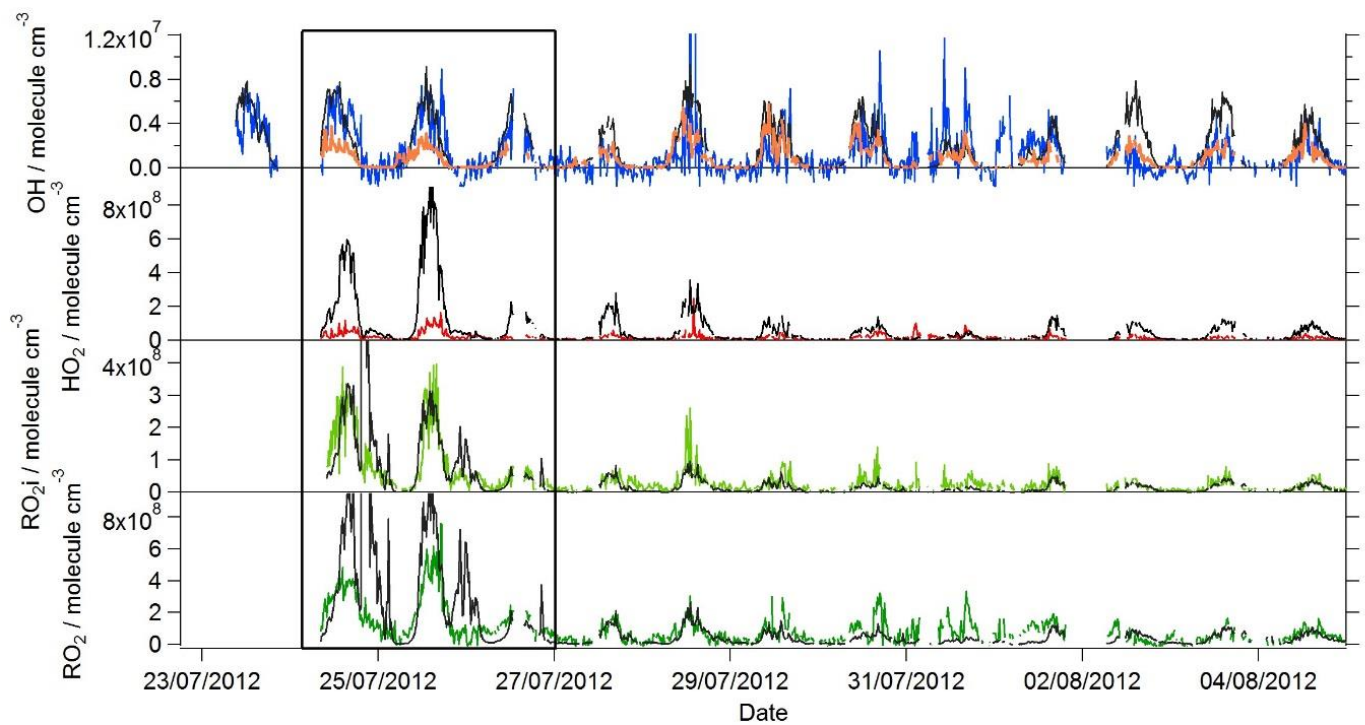
Figure 2: Observed (coloured lines) and MCM-BASE modelled (black lines) OH, HO₂, RO₂*i* and RO₂ during the summer ClearfLo IOP; steady state [OH] ([OH]ₚₛₛ) is displayed by the orange line. Periods of Easterly flow are highlighted inside the black boxes.
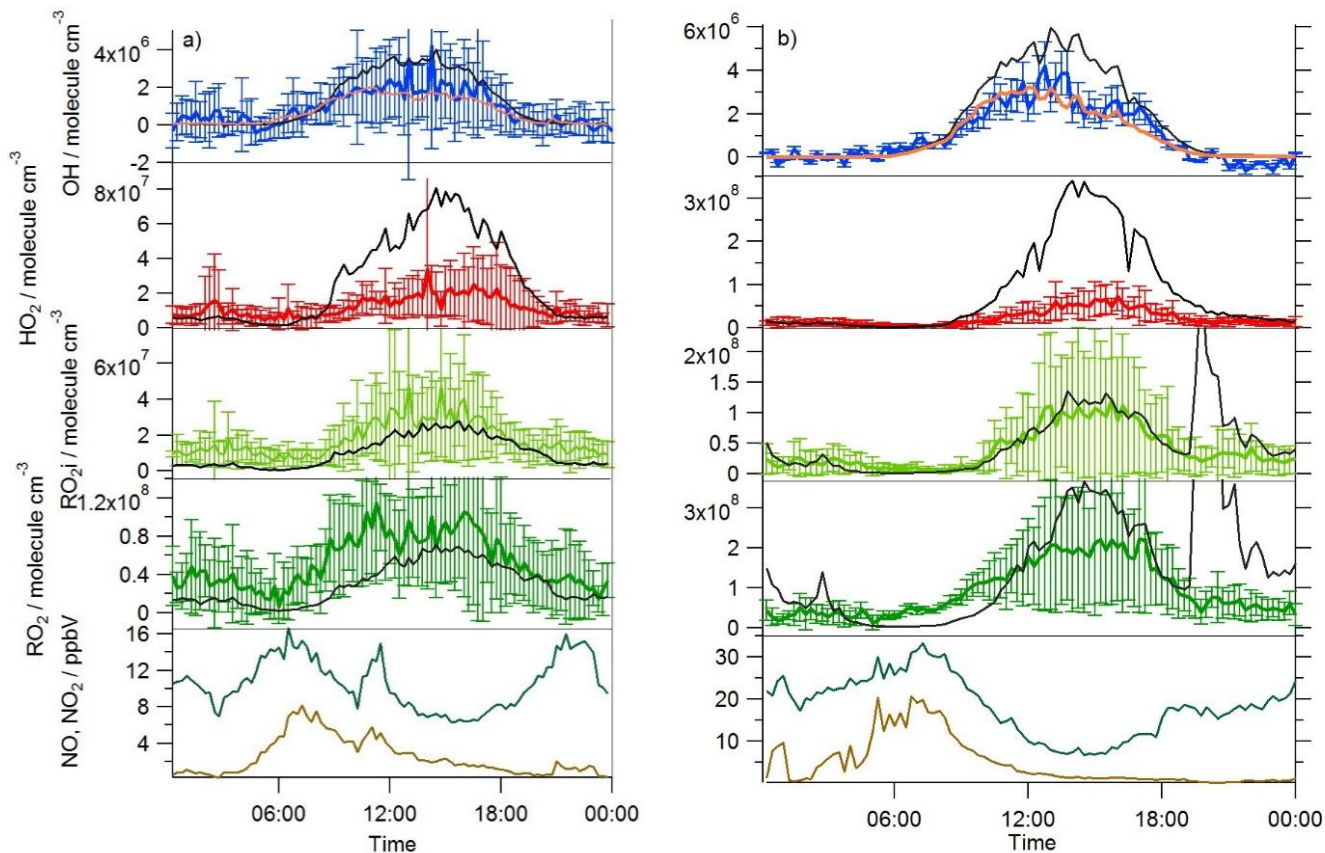
Figure 3: Average diel observed (coloured lines with error bars) and MCM-BASE (black line) OH, HO₂, RO₂*i* and RO₂ profiles during a) south-westerly and b) easterly flows; [OH]ₚₛₛ is displayed by the orange line. The error bars represent the 1σ variability in the observations. The average diel observed NO (brown line) and NO₂ (green line) are displayed in the bottom panels.
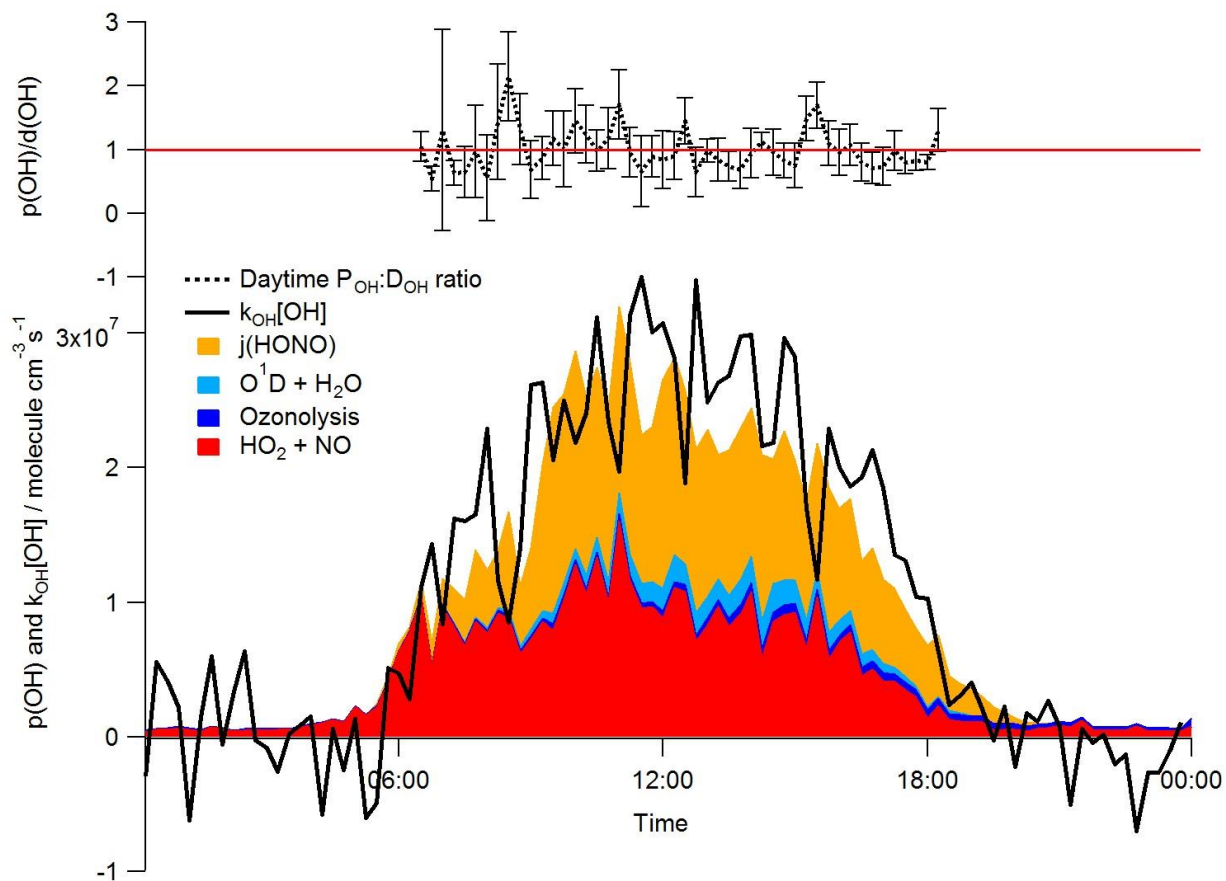
Figure 4: Median diurnal profiles for the whole campaign of the observed $D_{OH} = k_{OH} \times [OH]$. The summed rate of production of OH (P_{OH}) from the photolysis of HONO, the reaction of O(^{1}D) with H$_2$O, ozonolysis reactions and the reaction of HO$_2$ with NO is overlaid. The dashed black line represents the median daytime (06:30 – 18:30) $P_{OH} : D_{OH}$ ratio; error bars highlight the 1σ standard deviation of this ratio. The red line represents a ratio of 1.
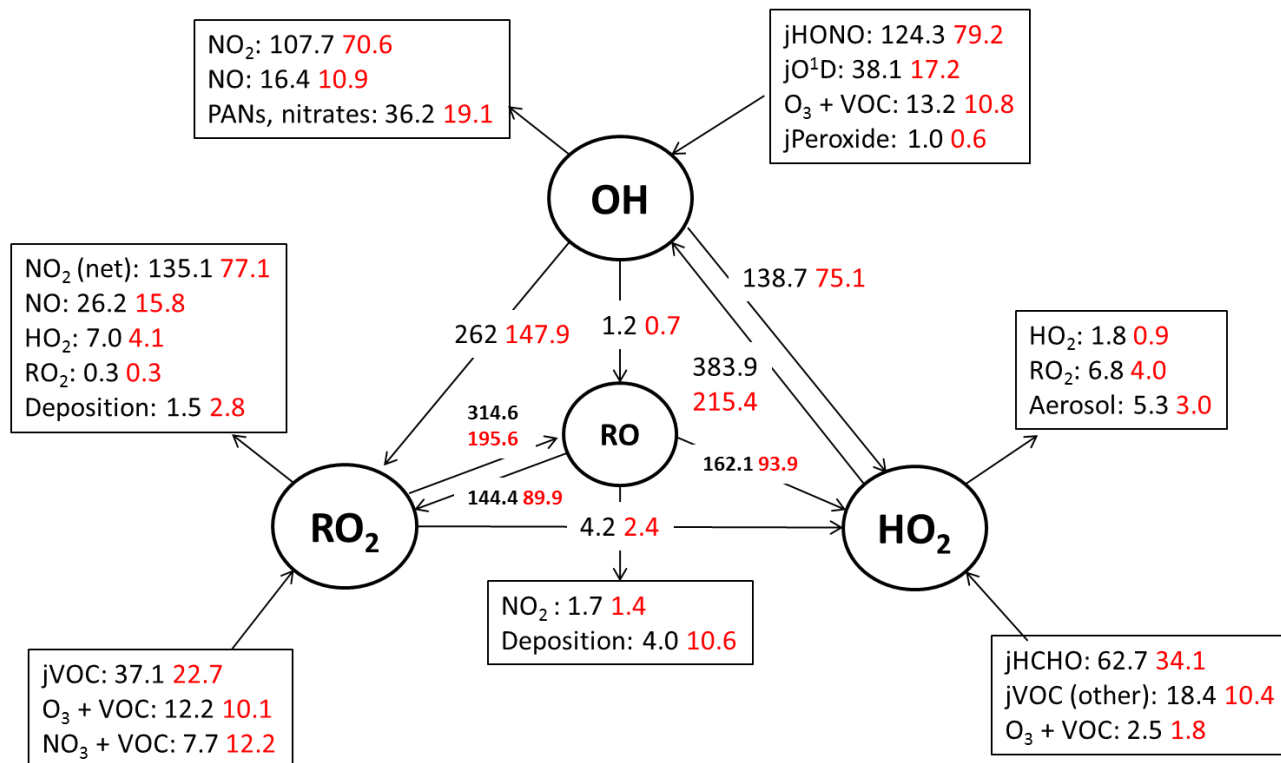
Figure 5: Mean daytime (11am – 3pm, black number and 6am – 9pm, red number) rates of reaction for formation, propagation and termination of radicals in units of 10^5 molecule cm^{-3} s^{-1} for the whole campaign period.
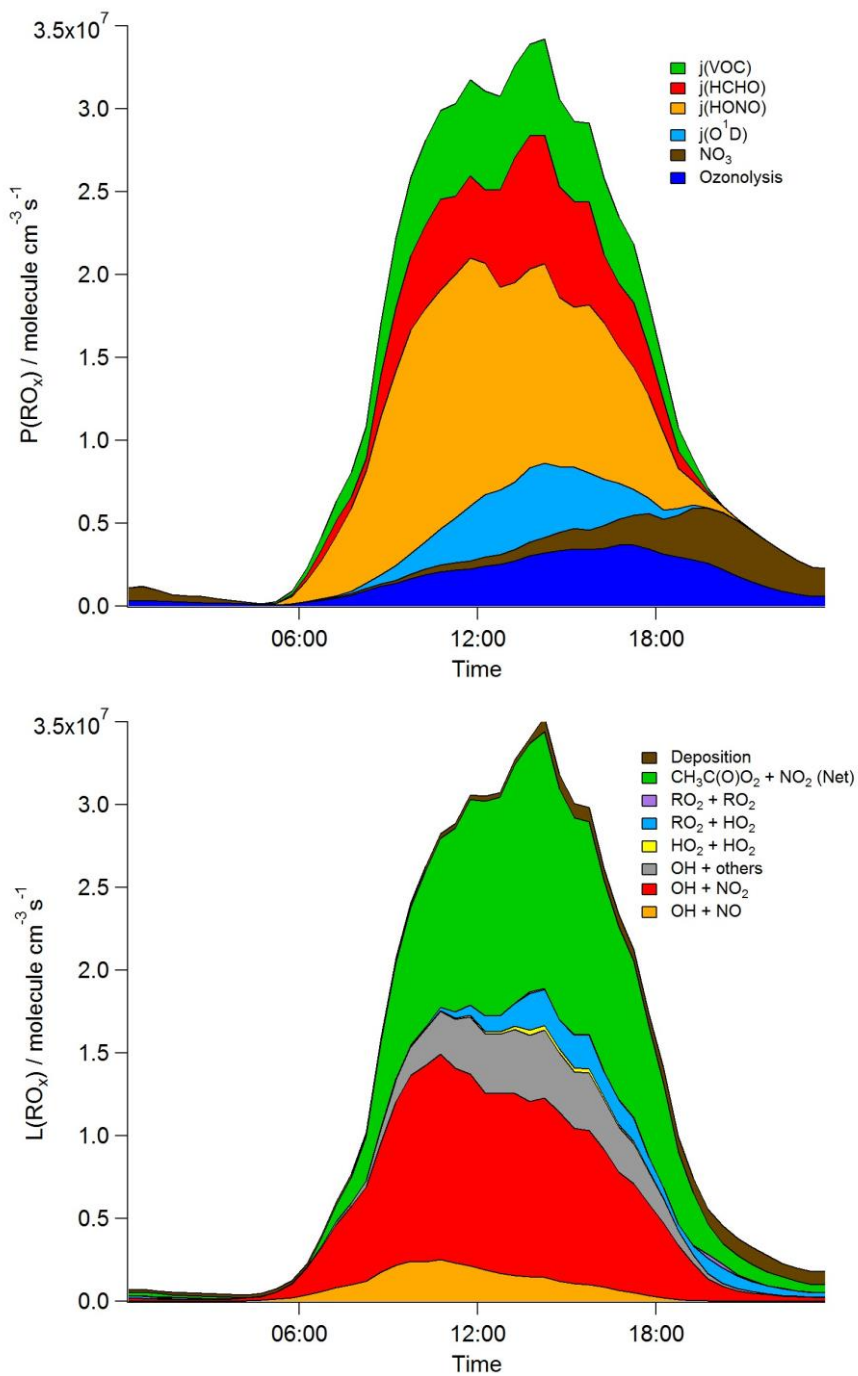
Figure 6: Mean diurnal profiles of MCM-BASE modelled rates of RO$_x$ initiation (upper panel) and termination (lower panel) reactions for the whole campaign period. 'CH$_3$C(O)O$_2$ + NO$_2$ (Net)' represents the net (forward - backward) CH$_3$C(O)O$_2$ + NO$_2$ ↔ PAN species.
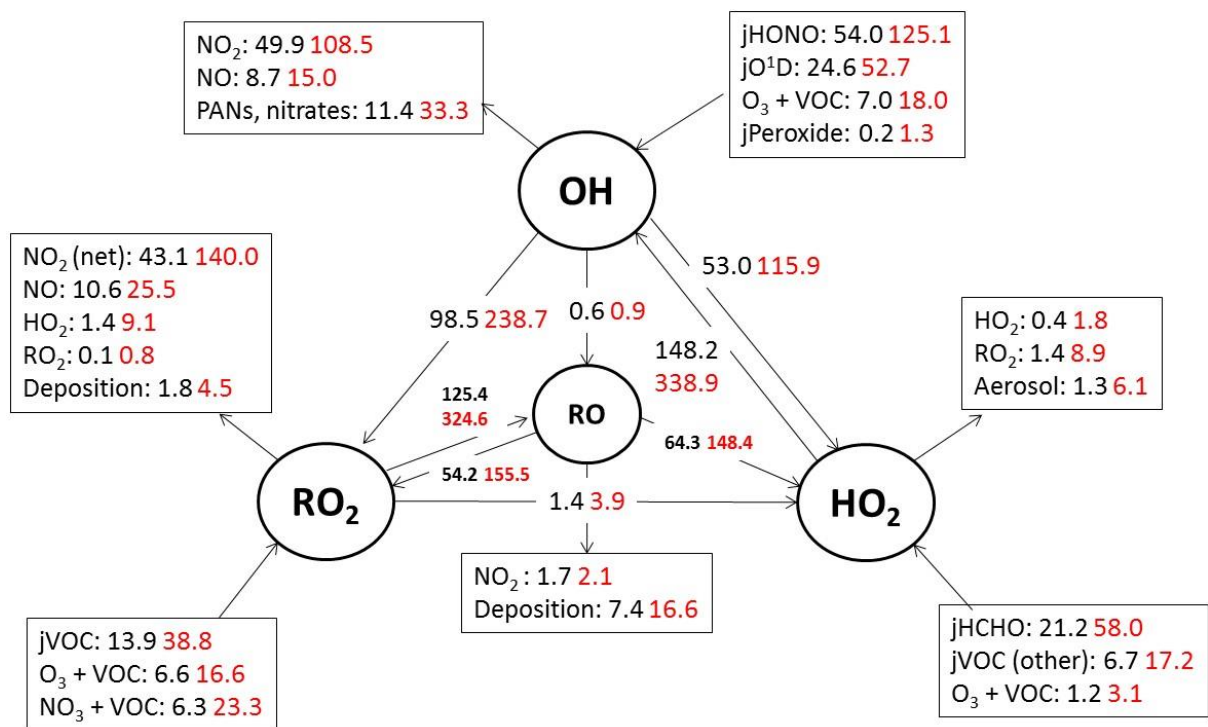
Figure 7: Mean daytime (6am – 9pm) rates of reaction for formation, propagation and termination of radicals in units of 10^5 molecule cm^{-3} s^{-1} for south westerly (black) and easterly (red) air masses.
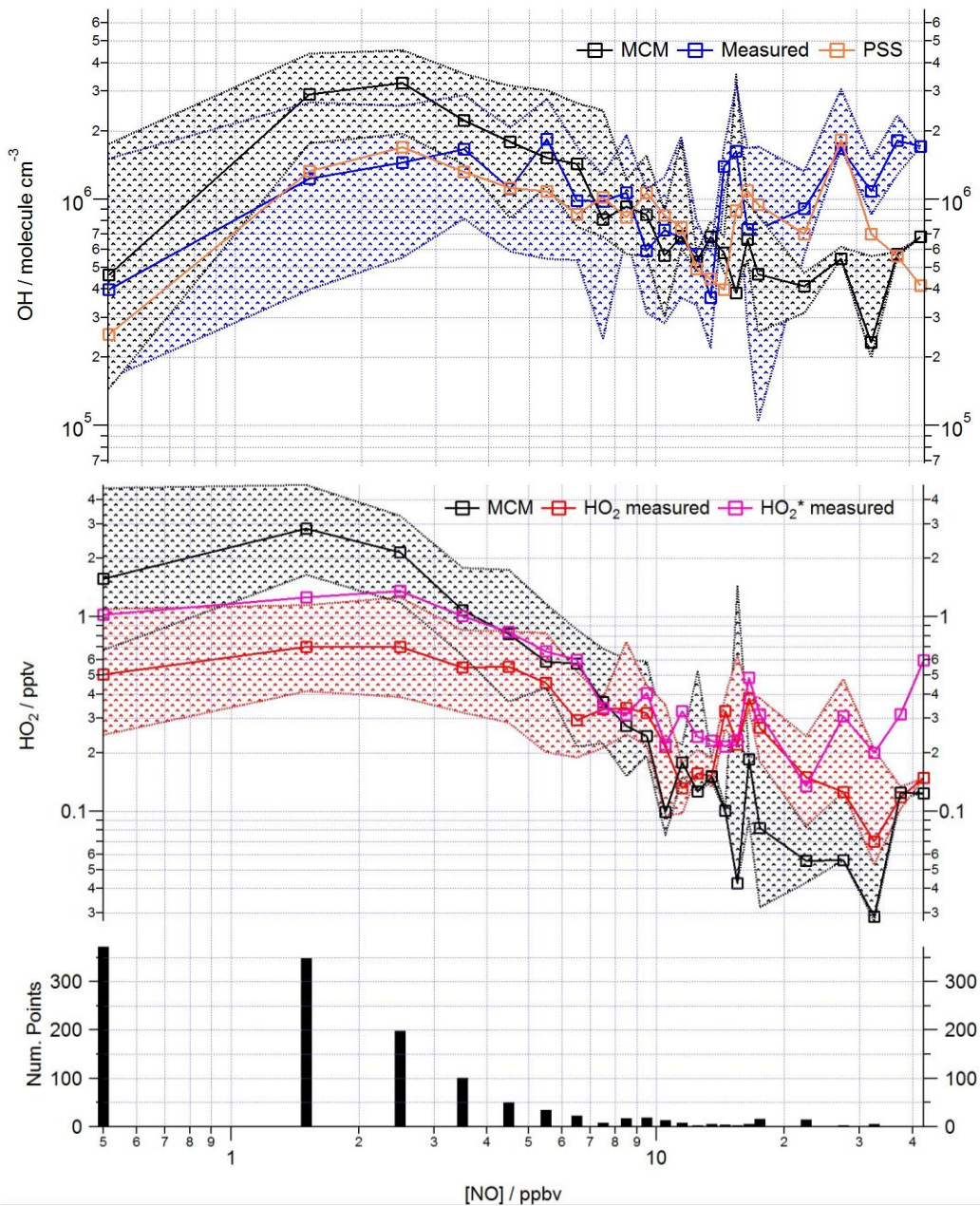
Figure 8: Observed and modelled HO$_x$ behaviour as a function of NO for the whole campaign period. (a) Median OH measured (blue squares), OH modelled (base MCM model = black squares, steady state calculation = orange squares). (b) Median HO$_2$ measured (red squares), HO$_2$* measured (pink squares), HO$_2$ modelled (black squares). Patterned areas represents the 25/75th percentiles. Data are filtered for daytime hours between 6 am and 7 pm and binned by [NO] with a bin width = 1 ppbv for [NO] between 0 – 20 ppbv and bin width = 5 ppbv for [NO] between 20 – 45 ppbv. The number of points in each bin is displayed in the lower panel.
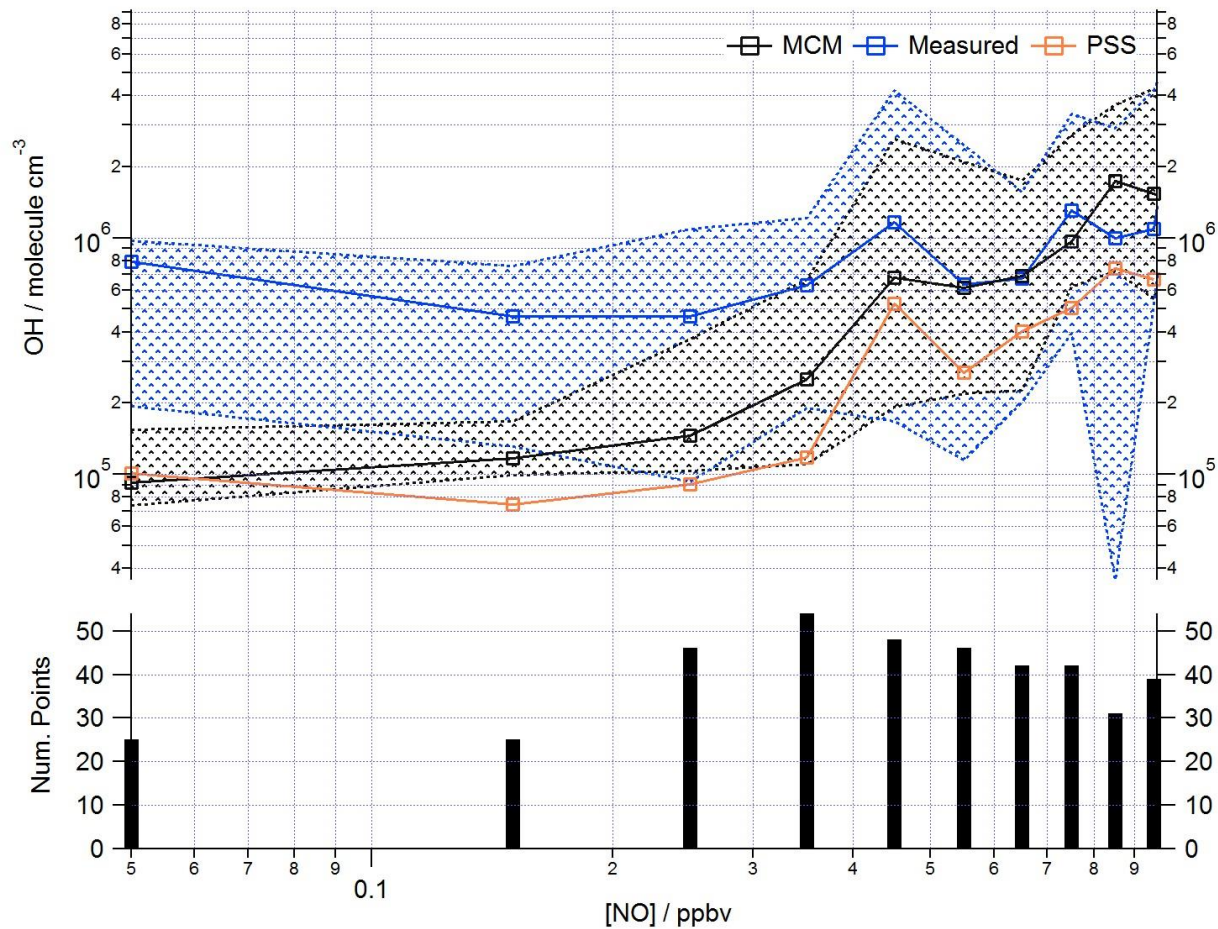
Fig 9: Observed and modelled OH behaviour as a function of NO (< 1 ppbv) for the whole campaign period. Median OH measured (blue squares), OH modelled (base MCM model = black squares, steady state calculation = orange squares). Patterned areas represents the 25/75th percentiles. Data are filtered for daytime hours between 6 am and 7 pm and binned by [NO] with a bin width = 0.1 ppbv. The number of points in each bin is displayed in the lower panel.
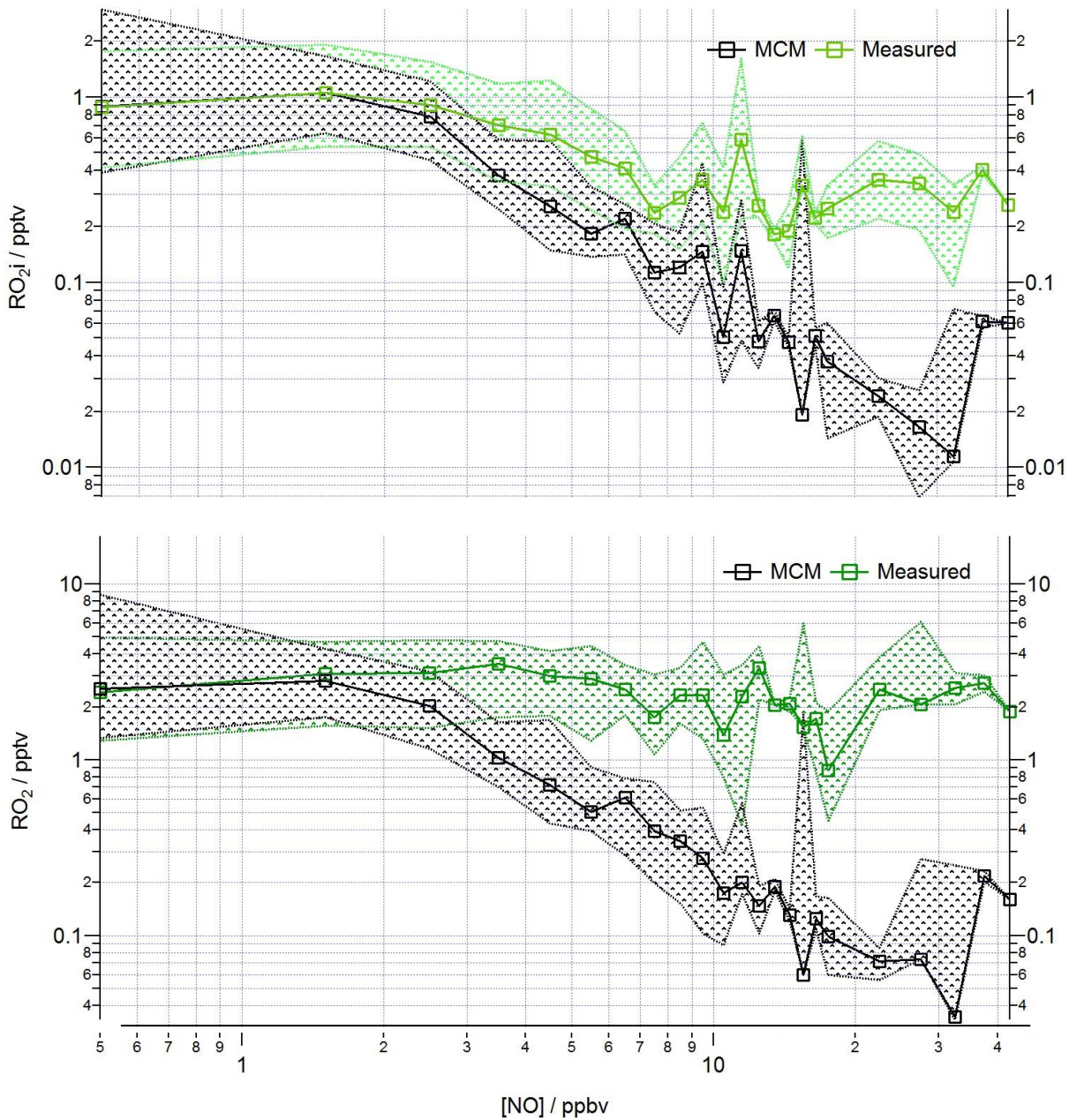
Figure 10: Observed and modelled RO$_x$ behaviour as a function of NO for the whole campaign period. (a) Median RO$_2$$i$ measured (green squares), RO$_2$$i$ modelled (black squares). (b) Median RO$_2$ measured (green squares), RO$_2$ modelled (black squares). Patterned areas represents the 25/75th percentiles. Data are filtered for daytime hours between 6 am and 7 pm and binned by [NO] with a bin width = 1 ppbv for [NO] between 0 – 20 ppbv and bin width = 5 ppbv for [NO] between 20 – 45 ppbv.
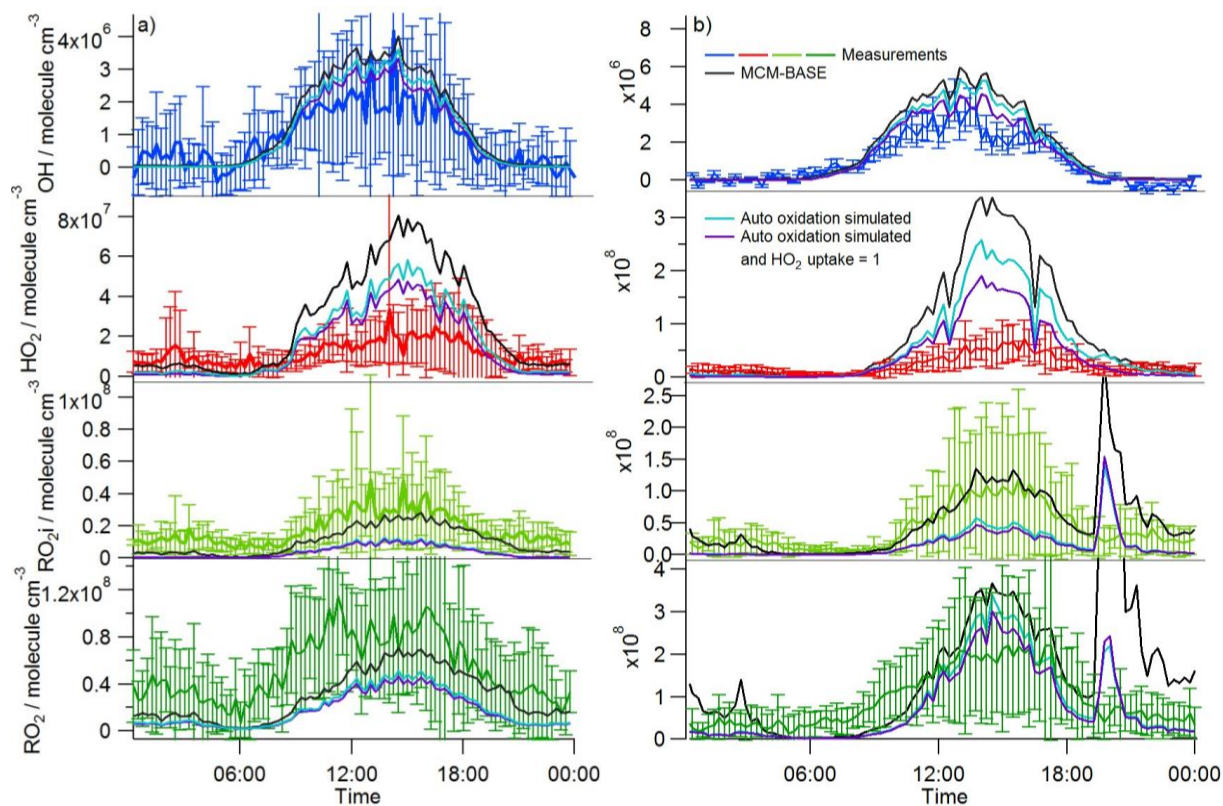
Figure 11: Average diel observed and modelled HOₓ profiles during a) south-westerly and b) easterly flows. The base model predictions are represented by the black line. The model scenario run with standard VOC species only and missing reactivity represented by converting OH to C6H5O2 is represented by the pale blue line; the purple line represents the model scenario run with standard VOC species only and missing reactivity represented by converting OH to C6H5O2 and an enhanced heterogeneous loss of HO₂, $\gamma_{HO_2} = 1$.
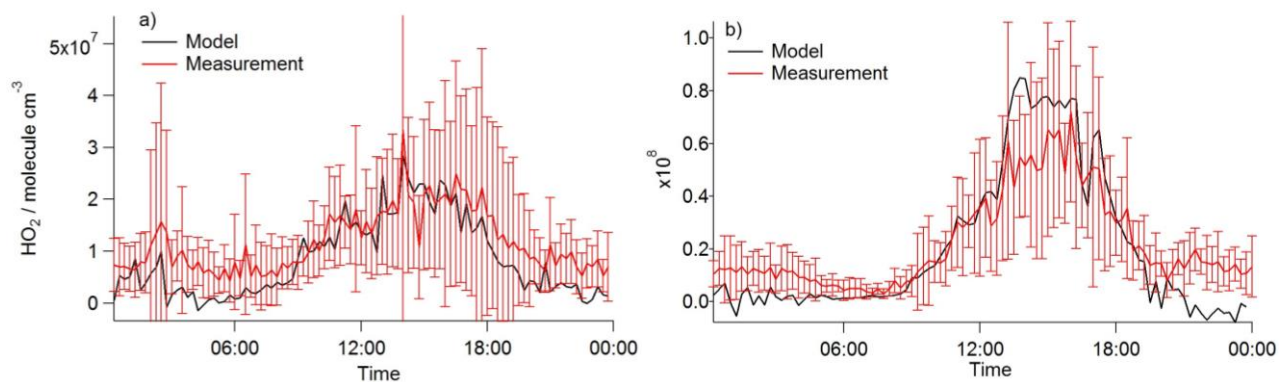
Figure 12: Average diel profiles of HO₂ concentration observed (red line with error bars) under a) south-westerly and b) easterly conditions. Overlaid is HO₂ calculated using the solution to the HO₂ quadratic expression (E7) (represented by the black line) with α equal to 0.15.
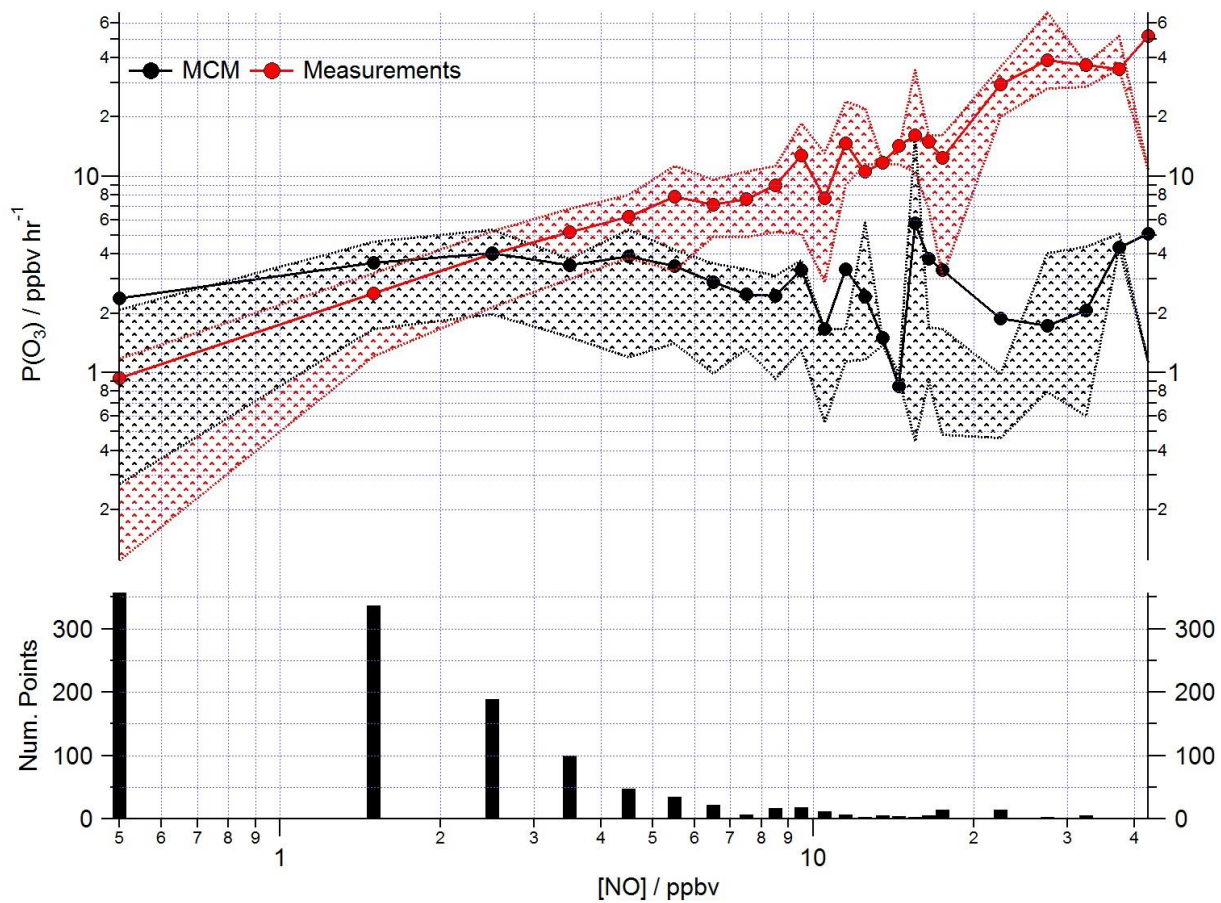
Figure 13: Mean ozone production (ppbv hr⁻¹) calculated from observed (red squares) and modelled (black squares) RO_x concentrations using E1 as a function of NO. Data are filtered for daytime hours between 6 am and 7 pm and binned by [NO] with a bin width = 1 ppbv for [NO] between 0 – 20 ppbv and bin width = 5 ppbv for [NO] between 20 – 45 ppbv.

Table 1: Relative efficiency of RO$_2$ to HO$_x$ conversion for different RO$_2$ species

Hydrocarbon	RO$_2$ relative sensitivity
Methane	1.0±0.03
Isoprene	1.0±0.05
Ethene	0.94±0.04
Toluene	0.88±0.05
Butane	0.78±0.03
Cyclohexane	0.79±0.02

Table 2: Listing of the concurrent measurements made during ClearfLo

Measurement	Instrument	Technique	LOD	Reference
O_3	Thermo 49i series	UV Absorption	0.05 ppbv	
CO	Aerolaser 5002	VUV-fluorimetry	1 ppbv	(Gerbig et al., 1999)
NO, NO_2	Air Quality Design Inc.	Chemiluminescence with LED NO_2 converter	1.8 pptv (NO), 5.5 pptv (NO_2)	(Lee et al., 2009)
HONO	LOPAP	Long-path absorption photometry	3 pptv (4 min)	(Heland et al., 2001)
PAN	GC-ECD	Gas chromatography with electron capture detection	5 pptv (90 s)	(Whalley et al., 2004)
HCHO	Aerolaser 4021 analyser	Hantzch reaction	<0.05 ppbv	(Salmon et al., 2008)
Actinic flux	Ocean optics QE65000	Spectrometer coupled to 2π quartz collection dome	-	
$j(O^1D)$	Meteorologie Consult	Filter radiometry	-	(Bohn et al., 2016)
C1-C8 hydrocarbons	(DC)-GC-FID	Dual-channel gas chromatography with flame ionisation detection	1 – 40 pptv	(Hopkins et al., 2003)
C6-C13 hydrocarbons	GCxGC-FID	2 dimensional gas chromatography with flame ionisation detection	0.01 – 0.2 pptv	(Lidster et al., 2014)
OH, HO_2, RO_2	FAGE	Laser induced fluorescence	See text	(Whalley et al., 2013)
k_{OH}	LP-LIF	Laser flash photolysis, laser induced fluorescence	2.1 s^{-1}	(Stone et al., 2016)
Meteorological parameters	Davis Vantage Vue	Met station	-	
Boundary layer depth	Halo-Photonics scanning Doppler lidar	Doppler lidar	30 m	(Barlow et al., 2015)
Aerosol surface area	TSI Inc, model 3321	Aerodynamic particle sizer spectrometer	0.001 particle/cm^3	(Peters and Leith, 2003)

Table 3: Model constraints and their average and maximum noontime concentrations during South westerly and Easterly flows

Species	Mean concentration / ppbV, South Westerly flow	Mean concentration / ppbV, Easterly flow	Max noontime concentration / ppbV, South Westerly flow	Max noontime concentration / ppbV, Easterly flow
Ozone	24.2	37.4	34.4	87.8
Nitric oxide	2.5	5.5	33.4	11.9
Nitrogen dioxide	10.6	18.8	101.6	39.3
Carbon monoxide	213.8	272.7	298.4	311.0
Nitrous acid	0.32	0.56	0.89	0.89
Nitric acid	0.67	1.54	1.59	3.89
Peroxyacetyl nitrate	0.07	0.23	0.09	2.63
Methanol	2.4	5.2	5.5	8.9
Ethanol	2.4	5.7	5.2	6.8
Propanol	0.3	0.64	0.83	1.5
Butanol	0.6	0.84	1.42	2.1
Methane	1853.0	1903.2	1939.0	1971.5
Ethane	3.1	6.8	4.6	6.0
Propane	1.2	2.7	3.1	3.6
i-Butane	0.5	1.1	1.5	1.8
n-Butane	1.0	2.2	2.9	4.3
i-Pentane	0.5	1.2	1.5	2.4
n-Pentane	0.2	0.6	0.6	1.0
Hexane	0.3	0.7	1.7	1.4
Heptane	0.2	0.4	0.5	0.5
Octane	0.1	0.3	0.5	0.4
2-Methyl pentane	0.2	0.3	0.5	0.8
Nonane	0.2	0.4	0.8	0.5
Decane	0.2	0.4	0.6	0.4
Undecane	0.3	0.7	1.0	0.6
Dodecane	0.6	1.3	2.4	1.3
Dichloromethane	0.03	0.06	0.08	0.09
Acetylene	0.3	0.5	0.9	0.8

Ethene	0.5	0.9	1.7	1.7
Propene	0.2	0.3	0.5	0.3
Trans-2-butene	0.02	0.03	0.04	0.05
But-1-ene	0.05	0.08	0.1	0.12
Metyl propene	0.04	0.07	0.1	0.1
Cis-2-butene	0.01	0.02	0.03	0.03
Pent-2-ene	0.02	0.04	0.06	0.06
Pent-1-ene	0.02	0.04	0.04	0.05
Trichloroethene	0.01	0.02	0.03	0.03
Benzene	0.12	0.2	0.3	0.3
Toluene	0.36	0.7	1.0	1.0
Ethylbenzene	0.06	0.1	0.2	0.2
1,3-Dimethylbenzene	0.04	0.08	0.1	0.1
1,4-Dimethylbenzene	0.04	0.08	0.1	0.1
1,2-Dimethylbenzene	0.05	0.11	0.1	0.2
1,2,3-Trimethylbenzene	0.01	0.01	0.04	0.02
1,3,5 -Trimethylbenzene	0.01	0.01	0.13	0.03
1,2,4-Trimethylbenzene	0.02	0.03	0.25	0.11
Phenylethene	0.02	0.05	0.06	0.07
1-Methylethylbenzene	0.002	0.003	0.01	0.01
Propylbenzene	0.03	0.09	0.17	0.24
3-Ethyltoluene	0.01	0.02	0.14	0.08
4-Ethyltoluene	0.01	0.02	0.07	0.05
2-Ethyltoluene	0.01	0.01	0.11	0.03
Benzaldehyde	0.01	0.01	0.03	0.06
α-Pinene	0.12	0.2	0.31	0.46
Limonene	0.04	0.07	0.12	0.23
Formalydehyde	6.7	13.8	10.1	29.9
Acetaldehyde	3.3	6.6	7.6	9.2
Acetone	2	3.4	3.7	5.3
Methacrolein	0.02	0.03	0.06	0.12
Methylvinylketone	0.02	0.04	0.07	0.13
2-Methylpropanol	0.04	0.06	0.1	0.2

Acetic Acid	0.04	0.06	0.1	0.2
Butan-2-one	0.05	0.08	0.14	0.25
n-Butanal	0.01	0.02	0.03	0.06
2-Penanone	0.02	0.04	0.07	0.13
n-Pentanal	0.02	0.03	0.06	0.1
4-Methyl-2-pentanone	0.04	0.07	0.12	0.23
Hexan-2-one	0.03	0.05	0.09	0.15
Cyclohexanone	0.01	0.02	0.04	0.08
1,3-Butadiene	0.01	0.02	0.05	0.02
Isoprene	0.1	0.2	0.3	0.48